Measurement and Analysis of Terminal Shock Oscillation and Buffet Forcing Functions on a Launch Vehicle Payload Fairing

David J. Piatak[1] Martin K. Sekula[2]
Aeroelasticity Branch / NASA Langley Research Center
Hampton, VA 23681

The buffet loads on a launch vehicle payload shroud can be impacted by the unsteadiness associated with a terminal shock at high subsonic speeds. At these conditions, flow accelerates to supersonic speeds on the nose of the payload fairing and is terminated by a normal shock on the cylindrical section downstream of the nose cone/cylinder shoulder. The location of the terminal shock and associated separated boundary layer is affected by the freestream Mach number, Reynolds number, and the pitch/yaw of the launch vehicle. Furthermore, even when the freestream conditions and vehicle attitude are constant, this terminal shock oscillates on the surface of the vehicle. The time-varying surface pressure associated with the terminal shock results in unsteady aerodynamic loads that may interact with vehicle structural dynamic modes and the guidance and control of the vehicle. Buffet testing of a 3-percent scale rigid buffet model of a launch vehicle cargo configuration with a tangent-ogive payload shroud was conducted in 2012 and in 2016. Initial buffet forcing functions (BFFs) utilized a coarse pressure sensor distribution on the vehicle surface in which a single longitudinal station with eight sensors observed the terminal shock environment at Mach 0.90. An examination of these circumferential pressures reveal large impulse-like pressure fluctuations and an asymmetry in pressure when the vehicle is at a nonzero angle of attack that result in high BFFs. Revisions to the shock integration region were made based on computational fluid dynamics and shadowgraph video of shock motion to better represent the BFFs and reduce the high loads resulting from this environment. To more clearly understand this terminal shock environment, a second wind tunnel test was conducted with a dense distribution of 256 sensors at the terminal shock location. These sensor arrays presents a unique opportunity to observe the unsteady terminal shock environment and to characterize the impact of various integration schemes on the BFFs. This paper presents a summary of the development of BFFs for this terminal shock and a detailed analyses of shock region pressure coefficients, coherence, BFFs, shock location time histories, and power spectral density to help guide development of BFFs for other launch vehicle test and analysis programs.

I. Nomenclature

C_p = Pressure coefficient
C_y = Normalized buffet forcing function; y-direction
C_z = Normalized buffet forcing function; z-direction
D = Diameter, in
F = Force, lbf
f = Frequency, Hz
fs = Full-scale quantity
L = Length, inches

[1] Research Aerospace Engineer, Aeroelasticity Branch, david.j.piatak@nasa.gov, Member AIAA
[2] Research Aerospace Engineer, Aeroelasticity Branch, martin.k.sekula@nasa.gov, Senior Member AIAA

L_c = Longitudinal coherence length, inches
ms = Model scale quantity
M = Mach number
p = Pressure, psf
q = Dynamic pressure, psf
Re = Reynolds number, per-foot or nondimensional based on 1st stage core diameter
rms = Root-mean-square; (0.5-60Hz only)
Sta. = Model or vehicle station identification number
T = Time, secs
V = Velocity, ft/s
α = Alpha; vehicle angle of attack, deg
β = Beta; vehicle side-slip, deg
δ = Delta; shock condition quantity; 0 to 1
Δ = Indicates fluctuating component only; mean removed prior to rms computation
γ^2 = Magnitude-squared coherence
Ψ = Psi; sensor azimuthal location; positive clockwise looking aft (nose to engines)

Acronyms

BFF = Buffet forcing function
CFD = Computational fluid dynamics
OML = Outer mold line
PSD = Power spectral density, units^2/Hz
RBM = Rigid buffet model
SLS = Space Launch System
TDT = Transonic Dynamics Tunnel

Notice to Readers

The predicted performance and certain other features and characteristics of the Space Launch System vehicle are defined by the U.S. Government to be Sensitive But Unclassified (SBU). Therefore, values in plots and figures have been removed or normalized to arbitrary values.

I. Introduction

Unsteady aerodynamic flows and the buffet environments caused by them are an important consideration in the structural design of a launch vehicle. Fluctuating pressures, which arise from high-speed flows on nose cones, interstage frustums, protuberances, and constant-diameter cylindrical tankage regions, can originate from many sources such as flow separation, flow reattachment, compression/expansion corner geometry, wake effects, turbulence, vortex shedding, and transonic shock oscillations. These buffet environments can generate large oscillatory forces on the vehicle and induce vehicle vibratory responses of primary bending modes and of secondary internal components such as engines and avionics.[1-4] A vehicle's trajectory conditions such as Mach number, side-slip angle, and angle of attack change rapidly during its climb to orbit, although the buffet environment is typically most severe within the transonic Mach range. Careful attention to the vehicle loads and dynamics is therefore required at these conditions during the design cycle and vehicle certification process. Transonic buffet loads have been linked to at least two launch vehicle failures in the past and are discussed in Ref. 5 by Fleming, which provides a concise overview of launch vehicle buffet.

To ensure positive structural margins for a launch vehicle, many load environments must be considered in the design to include loads arising from: liftoff, engine-induced vibrations, ignition overpressure, aeroacoustic high-frequency sound pressure, wind shear, turbulence, fuel/oxidizer slosh motion, staging events, vehicle maneuvers, steady aerodynamics, and buffet. Buffet loads arise from the vehicle's response to unsteady aerodynamic pressures on the vehicle surface, which are represented by time varying buffet forcing functions (BFFs). Vehicle BFFs are typically obtained via transonic/supersonic wind-tunnel testing of a rigid buffet model instrumented with hundreds of

unsteady pressure sensors located to reveal the peak buffet environments and provide adequate spatial resolution for BFF development. These buffet environments and all other load environments are applied to a detailed finite element model of the vehicle as part of the coupled loads analysis (CLA) process to determine the structural responses and vehicle structural safety margins.[6] The development of BFFs from wind-tunnel unsteady pressure measurements involve the application of basic integration schemes, sensor-to-sensor coherence analyses, attenuation of wind-tunnel facility acoustic tones, and the proper scaling to full-scale trajectory conditions. The BFF development processes are detailed in Refs. 7 through 9. Buffet test programs associated with the NASA Space Launch System (SLS) have been underway since 2011 and have delivered BFF databases for the Block 1 and Block 1B crewed vehicles and the Block 1B cargo vehicle.[10-12]

The degree of buffeting that a launch vehicle endures during transonic flight is highly dependent upon the shape of the vehicle. For cargo payload shrouds such as the 8.4 meter tangent-ogive shroud on the SLS Block 1B vehicle shown in Figure 1, a terminal shock or normal shock will be present at Mach numbers between approximately 0.85 and 0.95 on the cylindrical region of the payload shroud, downstream of the nose cone shoulder. The strength, location, and unsteadiness of this shock wave will vary with Mach number, vehicle attitude, Reynolds number, and dynamic pressure. Additionally, the terminal shock will interact with the local boundary layer and potentially cause flow separation downstream of the shock, particularly when coupled with downstream backward-facing frustums associated with changes in stage diameters or payload shroud interfaces. Figure 2 shows a shadowgraph of the terminal shock observed on a wind-tunnel model of the SLS Block 1B tangent-ogive payload shroud at Mach 0.90 and α=3.93°.

A terminal shock BFF presents a challenge to accurately assemble from a very limited spatial sensor density that is typical of most rigid buffet models. This fact proved itself true during the development of the SLS Block 1B cargo BFFs and resulted in preliminary terminal shock BFFs at M=0.90 that were overpredicted and resulted in negative structural margins for upper stage components. Subsequent revisions to the BFFs based on computational fluid dynamics (CFD) and shadowgraph observations at the terminal shock station reduced this buffet environment. However, the program requested increased confidence in the methods used to reduce the terminal shock BFF for loads cycle maturity for flight. Therefore, an additional transonic buffet test of this configuration was carried out with a very high spatial density of unsteady pressure measurements in the vicinity of the terminal shock. Two-hundred fifty-six sensors were arranged in longitudinal arrays of 16 ports at 16 equally-spaced azimuths at the terminal shock location of interest. Test results supported earlier efforts to reduce the terminal shock BFF and showed that greater reductions in BFF magnitude could be realized.

This paper will discuss the test and analysis program efforts to refine the BFF associated with an unsteady terminal shock on a tangent-ogive payload shroud at transonic conditions. A 3-percent scale model of the SLS Block 1B cargo configuration was tested at the NASA Langley Research Center Transonic Dynamics Tunnel (TDT) and is shown in Figure 3. Initial BFFs will be presented that utilized a single longitudinal station of eight unsteady sensors to observe the terminal shock, including revised BFFs based on these test data using CFD- and shadowgraph-derived longitudinal integration boundaries. Subsequent results and analysis of unsteady pressure data obtained from tests utilizing 256 unsteady measurements near the terminal shock will reveal a refined understanding of the buffet environment due to a transonic terminal shock. The analyses of shock region pressure coefficients, coherence, BFFs, shock location time histories, and power spectral density from these data will help guide development of BFFs for other launch vehicle test and analysis programs.

II. SLS Block 1B Cargo Buffet Test Program Description

Data presented in this paper are sourced from two SLS buffet wind-tunnel test programs that were conducted at the TDT in 2012 and 2016 using a 3-percent scale rigid buffet model. The TDT is a closed-circuit, continuous flow wind-tunnel that has been utilized for many recent buffet test programs including Ares/Constellation Ares I-X and Ares I, Dream Chaser Atlas V, and SLS. It has a 16- by 16-foot slotted transonic test section capable of reaching Mach 1.2 at a range of stagnation pressures from near vacuum to atmospheric pressure in both an air and R134a heavy-gas test medium. Dynamic pressures up to 300 psf and 550 psf can be attained in air and R134a, respectively.[13-15] Table 1 lists the TDT test conditions for several Mach numbers for the SLS buffet model testing. Additional technical details of the model design, instrumentation, and test program can be found in Refs. 10 through 12.

The 2012 buffet test program focused on both SLS crew and cargo configurations and included an early outer mold line (OML) definition of the SLS Block 1B cargo vehicle. This 2012 cargo configuration is shown mounted within the TDT test section in Figure 3 and possessed 472 unsteady pressure ports, which focused on the buffet environment of the entire vehicle including the left and right solid rocket boosters. This configuration possessed a coarse sensor

density of just eight ports located near the terminal shock at Mach 0.90. Figure 4 illustrates the unsteady pressure sensor distribution on the tangent-ogive payload shroud of the SLS cargo vehicle as tested in 2012. Station 5 in this figure is located near the terminal shock at Mach 0.90.

A second SLS Block 1B cargo vehicle test was conducted in 2016, which included updates to the model OML to represent the latest design of the vehicle including core and upper stage protuberances. Figure 5 shows the updated 3-percent scale SLS Block 1B cargo vehicle mounted in the TDT test section. The primary objective of this test was not the global vehicle buffet environment, but instead the refinement of the buffet environment specific to the terminal shock oscillation at Mach 0.90. The model shown in Figure 5 includes 16 azimuthal shock arrays containing 16 unsteady pressure transducers each for a total of 256 measurements to refine the buffet environment associated with the terminal shock at Mach 0.90. A detailed graphic of the shock array design is shown in Figure 6 and Table 2 lists the shock array longitudinal port station locations and azimuthal offsets from the array cardinal azimuth. Each of the 16 arrays are centered on an azimuth angle in increments of 22.5° starting at 0° and ending at 337.5° with positive azimuthal direction being defined as clockwise looking down the length of the vehicle (nose to engines). The 16 unsteady pressure ports in each array are located in two rows offset from the center of the array by +/-1° in order to provide adequate clearance for sensor installation. Each port is labelled 'a' through 'p' and the third port, port 'c', is at the same longitudinal station as station 5 from previous buffet testing. This high density of unsteady measurements was expected to provide the detail needed to resolve the questions that remained regarding the Mach 0.90 terminal shock BFFs generated using the coarse sensor distribution of the original rigid buffet model.

III. Terminal Shock BFFs Based on Coarse Sensor Distribution

Rigid buffet wind-tunnel models typically are limited to a sensor spatial density that fits within the limitations of facility data acquisition system channel count, model scale, and test program budget. When a limited pressure sensor spatial density is considered, there is a chance that the presence of the terminal shock is not observed by the sensors, unless the test matrix is carefully chosen. On the other hand, a ring of sensors may align with the terminal shock at a tested Mach number and reveal a highly nonlinear fluctuating pressure level associated with the supersonic and subsonic conditions upstream and downstream of the shock as it moves back and forth across the sensor ports.

A. Preliminary SLS Block 1B Cargo BFFs Based on Coarse Sensor Distribution

Figure 4 shows the unsteady buffet and aeroacoustic pressure sensor layout on the tangent-ogive payload shroud of the 3-percent scale SLS Block 1B cargo vehicle rigid buffet model as tested at the LaRC TDT in 2012. Station number 5 in this figure is near the longitudinal location of the terminal shock at approximately Mach 0.90. The pressure time history observed by sensors at the terminal shock location appear as a random square-wave signature as seen in Figure **7**, which shows pressure coefficient (C_p) versus time at a Mach number of 0.90 for a vehicle attitude of α=0° and 4°, and β=0°. The pressure sensed at this station fluctuates rapidly between a supersonic pressure (lower C_p) when the shock is downstream of station 5 and a subsonic pressure (higher C_p) when the shock is upstream of station 5. In contrast to the high spatial density results to be discussed later, the magnitude and frequency of the longitudinal oscillation of the terminal shock location cannot be obtained from analysis of these pressure signatures to aid in the development of BFFs. For the α=0° case shown in Figure **7**a, the pressure time histories appear nearly symmetric azimuthally about the ring of sensors at 0°, 90°, 180°, and 270°. With the model pitched to α=4°, the pressure signatures in Figure **7**b no longer appear azimuthally symmetrical. When these pressures are integrated azimuthally and longitudinally to yield BFFs, the azimuthally asymmetric pressures in Figure **7**b result in very high BFFs for the terminal shock.

During development of preliminary BFFs for the SLS Block 1B tangent-ogive payload shroud, standard integration regions and coherence factor methods described in Refs. 8 and 9 were employed to generate full-scale normalized force time histories of BFFs from the raw pressure time histories. Table 3 lists the rigid buffet model scaling laws utilized in the scaling of model-scale parameters to full-scale parameters and Table 4 lists the full-scale reference trajectory conditions used for scaling. Figures 8 and 9 show the root-mean-squared (rms) levels for the y-direction and z-direction normalized full-scale BFFs ($\Delta C_{y,rms}$ and $\Delta C_{z,rms}$) for Mach numbers of 0.80, 0.90, 0.95, 1.10, and 1.18 at α=0° and 4°, and β=0°. Peak buffet environments are noted in each of these figures, which includes the terminal shock oscillation buffet environment at Mach 0.90 and the buffet environment caused by the booster forward attachment shed vortices at Mach 0.95. The booster forward attachment strut environment is fully documented in Ref. 12. For the case of α=0° and β=0° shown in Figure 8, the peak terminal shock environment is shown to be approximately the same magnitude for $\Delta C_{y,rms}$ and $\Delta C_{z,rms}$. However, when the vehicle is pitched to α=4° as shown in Figure 9, $\Delta C_{z,rms}$ is significantly higher and dominates the buffet environment given the nominal integration region boundaries as assumed in the preliminary analysis assumptions. The reason for this higher BFF rms level in the z-

direction is due to the azimuthally asymmetrical pressure signature observed by the station 5 ring of pressure sensors as shown in Figure 7b.

Longitudinal and azimuthal coherence was considered in the integration of pressures when developing the coherence-adjusted BFFs as described in Refs. 8 and 9. For the preliminary BFFs discussed above, special consideration for the terminal shock was not taken. Using the traditional coherence length analysis, coherence between longitudinal stations is computed and the mean coherence is computed for a desired frequency range. Mean coherence squared (γ^2) is then plotted versus the longitudinal separation distance between stations and a least-squares weighted exponential fit is applied to the data. Figure 10 shows the longitudinal coherence between all sensor station combinations plotted versus separation distance for stations 1-7 on the SLS Block 1B tangent-ogive payload shroud. The resulting coherence length for this region is also shown in this figure (104.5 inches full-scale) and is defined as the separation distance at which the weighted coherence curve fit is equal to 0.5. Using this coherence length for the payload shroud region, an effective coherence length is computed for each station and is compared in Figure 11 to the full zonal integration length for each station on the payload shroud for Mach 0.90 and α=0° and β=0°. As can be seen, the effective integration length for station 5 is not significantly lower than the zonal length and the terminal shock pressure signatures are being integrated over nearly 94-percent of the station 5 zonal length of 119.4 inches.

When these preliminary BFFs were utilized by the Marshall Spaceflight Center (MSFC) structural loads and dynamics team as part of the vehicle coupled loads analysis (CLA), the high terminal shock environments were determined to be the main contributor to negative structural margins on secondary structure including the 'hung stage' RL10C exploration upper-stage (EUS) engines. Thus, an effort was enacted to address these high loads with the emphasis on the fact that employing the full geometric integration region for station 5 was likely resulting in an overprediction of this terminal shock environment at Mach 0.90.

B. Revised SLS Block 1B Cargo BFFs Based on Coarse Sensor Distribution

Due to the large BFF magnitudes at the terminal shock location at Mach 0.90 and subsequent review of the resulting buffet load responses of the EUS engines, an effort was initiated to logically reduce these BFFs using available wind-tunnel data and CFD results. The obvious approach was to limit the longitudinal integration length associated with station 5 due to the large and localized pressure fluctuations observed by the sensors as the shock traversed back and forth across the station.

Both unsteady FUN3D CFD results and shadowgraph video data were utilized to estimate the footprint of the longitudinal extent of the terminal shock oscillation. Figure 12 shows a color intensity image of the standard deviation of each pixel from the shadowgraph video for the Mach 0.90, α=4°, and β=0° condition. By referencing known lengths of components in the field of view in Figure 12, the shock oscillation footprint was estimated to be 42 inches. Figure 13 shows FUN3D $C_{p,rms}$ results for Mach 0.90 for the SLS Block 1B tangent-ogive payload shroud. This simulation utilized a 35M tetrahedron mesh and the time-accurate run spanned 1.4 seconds at TDT wind-tunnel test conditions and is further discussed in Refs. 16 and 17. The peak region of $C_{p,rms}$ shown in Figure 13 illustrates the extent of the oscillation and effects of the terminal shock at Mach 0.90 near station 5 on the rigid buffet model. These results show the terminal shock footprint associated with the highest $C_{p,rms}$ mean longitudinal extent to be approximately 8.7 inches (full-scale) as shown in Figure 13. Based on the azimuthal excursions of peak $C_{p,rms}$, the more conservative extent of terminal shock footprint based on CFD appears to be approximately three times 8.7 inches or 26.1 inches. Given these two results from shadowgraph video data and FUN3D, 42 inches was chosen to be the longitudinal length of 'segment b' depicted in Figure 13 to represent the oscillation footprint (effective coherence length) of the terminal shock.

The revised BFFs representing the Mach 0.90 terminal shock were developed using a composite of forcing functions from stations 4, 5, and 6. Segment 'a' in Figure 13 is 46.5 inches long, segment 'b' is 42 inches as discussed above, and segment 'c' is 31 inches long. Pressure time histories from station 4 are applied to segment 'a' and station 6 pressure time histories are applied to segment 'c'. The terminal shock oscillation pressure signatures shown in Figure 7 are applied to the 42-inch terminal shock footprint in segment 'b'. These segment BFFs are summed together to obtain the final BFF time histories for the station 5 terminal shock. Figures 14 and 15 present preliminary BFFs and those with the revised station 5 composite BFF for a Mach number of 0.90 at α=0° and 4°, and β=0°. The reductions in station 5 terminal shock based on shadowgraph and FUN3D results are apparent and significant for this condition. However, questions remained regarding the confidence in these methods to represent the terminal shock and a test program was conducted to explore the buffet environment associated with the terminal shock for this vehicle configuration to ensure flight safety.

IV. Analysis of Terminal Shock Buffet Environment

Although the revised terminal shock BFFs for Mach 0.90 were shown to be lower using the composite forcing functions discussed above and the resulting buffet loads associated with the RL10C upper-stage engine were reduced, a buffet test – focused on this terminal shock environment region – was warranted to increase the program's confidence in BFFs, predicted buffet loads, and resulting structural margins. Modifications were made to the 3-percent scale SLS rigid buffet model Block 1B cargo configuration to include a very high density of unsteady pressure measurements at the location of the terminal shock at Mach 0.90 (station 5). As discussed in Section II, 16 azimuthally-spaced shock arrays were installed in the model. Each shock array had 16 unsteady pressure transducer ports arranged longitudinally and were offset +/-1° from the array cardinal azimuth for transducer mount clearance considerations. A total of 256 unsteady pressure transducers provided a unique opportunity to study the buffet environment and BFFs associated with an unsteady terminal shock on a launch vehicle payload shroud. Figure 5 shows the SLS model mounted in the TDT test section with shock arrays visible and Figure 6 shows details of the shock array design. Table 2 lists shock array port locations and azimuthal offsets.

A. Characteristics of the Terminal Shock on Block 1B Cargo Tangent-Ogive Payload Shroud

The sensitivity of shock location to flight conditions is of interest in generating BFFs associated with the shock oscillation buffet environment. Testing of the modified SLS cargo model at TDT included a finely-spaced transonic Mach range to identify the location of the shock on the shock array. Figure 16 presents mean pressure coefficient (C_p) distributions on the shock arrays at Mach numbers of 0.80, 0.85, 0.87, 0.90, 0.91, 0.92, 0.93, 0.94, and 0.94 and a vehicle attitude of α=0° and β=0°. This figure includes all 16 shock arrays at azimuth locations of 0° to 337.5° in 22.5° increments and the y-axis label of each plot lists the shock array cardinal azimuth. As can be expected for this zero total-α condition, the C_p distributions at each Mach number are consistently symmetric around the circumference of the payload shroud. Additionally, the transition from supersonic C_p (~0.6) to subsonic C_p (~0.1) is clearly seen for Mach numbers of 0.90, 0.91, and 0.92, which indicates the presence of the terminal shock on the sensor array. The shock is upstream of the shock array at Mach numbers of 0.80, 0.85, and 0.87 and downstream of the array at Mach 0.94 and 0.95. For Mach 0.93 (blue, right-pointing triangles), Figure 16 shows that the shock is located near the end of the array and partially downstream of the last port on the array.

Further insights regarding the terminal shock location and the extent of shock motion can be determined from a review of the fluctuating pressure at each port by computing the root-mean-square of the port pressure with the mean pressure subtracted ($\Delta C_{p,rms}$) as shown in Figure 17. The trends in $\Delta C_{p,rms}$ are shown to be symmetric and nearly identical for all sixteen shock arrays around the azimuth and the peak value being approximately 0.15 for the Mach 0.90 case. The peak value of $\Delta C_{p,rms}$ is shown to decrease with increasing Mach number from a value of 0.15 at Mach 0.90 to $\Delta C_{p,rms}$=0.11 for Mach 0.93. The array station at which the peak occurs is shown to shift downstream with increasing Mach number. As shown in Figure 16 and confirmed in Figure 17, the center of the shock footprint appears to be at the downstream end of the shock array at Mach 0.93. The terminal shock appears to be centered on the shock array at Mach 0.91 at approximately station 1460 inches, as shown in Figure 17.

As the vehicle pitch attitude is changed, the terminal shock footprint on the vehicle will not be symmetric. This is shown in data from the shock array in Figures 18 and 19, which presents $C_{p,mean}$ and $\Delta C_{p,rms}$ at a Mach number of 0.91, α=-6° to +6°, and β=0°. With respect to the centered terminal shock position for α=0° at approximately station 1460 inches found in Figure 19, the shock footprint on the top of the vehicle (Ψ=0°) is seen to move forward with increasing α and the shock footprint on the bottom of the vehicle (Ψ=180°) is seen to move aft with increasing angle of attack. On the sides of the vehicle at Ψ=90° and Ψ=270°, the shock location is unaffected by vehicle pitch change, as expected. These data clearly shows the impact of vehicle attitude on the location of terminal shock on OML surface and provides insight into the asymmetric nature of the shock at nonzero vehicle attitudes.

B. Estimation of Terminal Shock Time History

Given the high longitudinal pressure port density for this test configuration, it is possible to estimate a time history of the centroid of the terminal shock on the vehicle and more clearly define the shock oscillation footprint. Examination of histograms of the C_p time histories reveals the range of pressure coefficient values observed by the pressure ports on the shock arrays. Histograms shown in Figure 20 for the shock array at Ψ=90° clearly shows peaks associated with port locations that are predominantly measuring a supersonic C_p and those measuring a subsonic C_p. Summing the 16 C_p histograms shown in Figure 20 yields the summed histogram in Figure 21, which includes a polynomial fit of the histogram to enable computation of a supersonic and subsonic threshold pressure coefficient ($C_{p,supersonic}$ and $C_{p,subsonic}$) values for determination of shock location. The threshold C_p values are computed based

on locating the local maxima of summed histogram curve fit and using a reasonable curve fit slope to locate the supersonic and subsonic C_p values that bound the transition C_p region. This transition C_p region is the range of values shown in Figure 21 at which the measured port is in transition from a supersonic to subsonic (and vice versa) condition: the shock is just upstream or downstream of the measurement port on shock array. This concept of shock location and transition region with respect to the shock array measurement ports is shown in Figure 22. With flow on the array passing from left to right in Figure 22, the shock is located at an instant in time between ports 'h' and 'i', and ports 'a' through 'g' observe supersonic flow, while 'j' through 'p' observe subsonic conditions. Ports 'h' and 'i' will theoretically observe a pressure coefficient that is in the transition region of Figure 21 because the shock does not affect an infinitely narrow region in the direction of flow. However, from experience and an understanding of the physics of the flow in this region, we will see that many more ports are within the transition region.

Given the shock transition region defined in Figure 21, the time histories of C_p for measurement ports 'a' through 'p' can be interrogated to determine a shock condition between 0 and 1. This shock condition, δ, is defined as,

$$\delta = 0 \text{ ; subsonic condition, } C_p \geq C_{p,subsonic}$$

$$\delta = \frac{C_{p,subsonic} - C_p}{C_{p,subsonic} - C_{p,supersonic}} \text{ ; transition condition, } C_{p,supersonic} < C_p < C_{p,subsonic}$$

$$\delta = 1 \text{ ; supersonic condition, } C_p \leq C_{p,supersonic}.$$

For each time step, a shock condition, δ, is computed for each port on each shock array based on the measured C_p value and the threshold C_p values computed from the curve fit to the array summed histograms, akin to that found in Figure 21. Figure 23a and 23b present pressure coefficient and shock condition time histories for the Ψ=90° shock array for a Mach number of 0.91 at ports 'a' through 'm', which span the supersonic to subsonic conditions. Pressure ports 'a' and 'b' are noted to be at predominantly supersonic C_p values throughout the time history and pressure ports 'k' through 'm' are noted to be predominantly subsonic. Between ports 'c' through 'j', the measured pressure coefficient is seen to rapidly transition between supersonic and subsonic states, which is indicative of the terminal shock rapidly moving longitudinally back and forth across the ports. At any instant in time, an estimate of the location of the shock can be determined with knowledge of the port locations and by examining the shock condition. It is assumed that the shock centroid corresponds to a shock condition value of 0.5. At an instant in time of 2-seconds for the time histories shown in Figure 23, the shock condition can be plotted versus port location as shown in Figure 24 and the shock centroid location can be interpolated between sensor stations to the shock condition value of 0.5. For this time instant, the shock centroid is at station 1464.1 inches (full-scale). Performing this analysis for multiple shock arrays for the entire time history length, we arrive at the full-scale shock centroid time histories shown in Figure 25 for the arrays at Ψ=0°, 45°, 90°, 135°, 180°, 225°, 270° and 315°. Mean and peak-to-peak magnitudes of shock location are shown to the left of each time history and reveal a range of mean and peak-to-peak magnitudes of between 1457.1 and 1458.0 inches and 40.6 and 49.2 inches, respectively.

The dominant frequencies of shock motion are of interest to BFF development and understanding of the terminal shock dynamics. Power spectral densities of shock position on the arrays at Ψ=0°, 90°, 180°, and 270° are shown in Figure 26, which reveals a broad peak located at 0.69 Hz. Also plotted in Figure 26 are power spectral densities of y-direction and z-direction accelerometers that were located in the payload shroud of the SLS wind-tunnel model. This data show peaks of 0.57 Hz in the y-direction and 0.40 Hz in the z-direction, which correspond to the first two model fundamental modes of vibration on the TDT support sting for full-scale trajectory conditions. Vibration tap tests were conducted on the model prior to testing and revealed first lateral and vertical bending modes associated with the model/sting to be at 9.8 Hz and 6.9 Hz, respectively, which correspond to the peaks at full-scale frequencies noted in Figure 26 for the accelerometers. Although the shock location and model accelerometer frequency peaks do not align, the terminal shock dynamics may be impacted by the model motion and/or facility turbulence/noise.

Computing shock condition and location analyses for an angle-of-attack sweep of -6°, -4°, -2°, 0°, +2°, +4°, and +6° at Mach 0.91 reveals the mean centroid location and extent of motion trends of the shock on each of the arrays as shown in Figure 27. These plots reveal that the mean shock location and extent of motion is highly dependent on vehicle orientation. For positive α, the shock location moves upstream toward the nose on the leeward or top of vehicle (Ψ=0°) and moves downstream on the windward or bottom of vehicle (Ψ=180°). The opposite trend is shown

for negative angles of attack in Figure 27. Examining the trends of the shock centroid location with α show that the shock footprint is quite sensitive to vehicle orientation. The extent of shock centroid motion (peak-to-peak magnitude) shown in Figure 27 indicates that, it too, is sensitive to vehicle orientation with the magnitude of motion ranging from 32 inches to as high as 58 inches. This extent of motion supports the conclusion reached in Section III-B to use a shock footprint width of 42 inches estimated by the shadowgraph and CFD analyses for use in revising the integration length for the shock station BFF.

C. Longitudinal and Azimuthal Coherence of Shock Array Pressure Time Histories

The coherence between pairs of pressure time histories is a useful tool in determining integration lengths and angles in regions of coarse sensor density. Buffet forcing functions presented in Section III were developed using coherence-based integration factors determined using the methods presented in Refs. 8 and 9 and intended to adjust the effective integration region to estimate the temporal and spatial effects of fluctuating pressures. These methods are used to reduce the anticipated conservatism and overprediction of BFFs that would result if the measured fluctuating pressures were integrated over its entire geometric region. However, the high sensor density for the shock arrays shown in Figure 6 was expected to preclude the need to apply a coherence-based integration factor for the development of the terminal shock BFFs.

Longitudinal and azimuthal magnitude-squared coherence, γ^2, versus full-scale separation distance and separation angle are shown in Figures 28 and 29 for a Mach number of 0.91 and vehicle attitudes of α=-6°, -4°, -2°, 0°, +2°, +4°, and +6°, and β=0°. Longitudinal magnitude-squared coherence in Figure 28 is computed between port 'a' and each subsequent downstream port on each azimuthal shock array. Azimuthal magnitude-squared coherence shown in Figure 29 for each azimuth location at a common longitudinal station is computed using the port at Ψ=0° as a reference. Sensor-to-sensor coherence values are shown to remain above or near a value of γ^2 = 0.5 for longitudinal separation distances greater than the sensor spacing of 5 inches, which suggests full longitudinal correlation of the pressure signal on the shock arrays. Studying the azimuthal magnitude-squared coherence shown in Figure 29, a similar result is found. Magnitude-squared coherence values greater than or near γ^2 = 0.5 are found for separation angles slightly greater than the azimuthal separation distance between shock arrays of 22.5°. Thus, the development of terminal shock BFFs using the shock arrays will assume that the measured pressures at each array port are fully correlated on each port's geometric patch and there is no need to apply a coherence-based integration factor to reduce integration areas.

V. Terminal Shock BFFs Based on Fine Sensor Distribution

The ultimate intent of modifying the SLS Block 1B cargo configuration's payload shroud to include 256 unsteady measurement ports focused on the terminal shock environment was to validate the assumptions used in BFF development discussed in Section III-B and to provide updated and more accurate terminal shock BFFs for this configuration. Buffet forcing functions for the terminal shock have been developed based on the shock array pressure port data and will be compared to the preliminary and revised BFFs discussed in Sections III-A and III-B. Additionally, sensitivity of BFFs to sensor location choice with respect to shock location will be discussed. Both root-mean-squared and power spectral densities of BFFs will be discussed and compared.

A. Terminal Shock BFFs Based on Integration of Individual Shock Array Sensor Stations

Sixteen terminal shock BFFs have been computed using the methods described in Refs. 8 and 9 at each shock array station ('a' through 'p') shown in Figure 22. The integration boundaries were defined using the longitudinal and azimuthal midpoint locations between sensors based on the array geometry listed in Table 2. Based on the high longitudinal and azimuthal coherence on the arrays shown in Figures 28 and 29, no coherence factors were applied and measured pressures were integrated over the full geometric boundaries. To arrive at a summed shock array BFF for comparison to the BFFs generated using the coarse sensor distribution shown in Figures 14 and 15, the BFF time histories at array stations 'a' through 'p' were summed at each time step. This 'summed BFF', representing the terminal shock BFF, is assumed to act at the longitudinal center of the shock array (between port 'h' and 'i'). Figure 30 presents root-mean-squared normalized BFF results at 16 shock array longitudinal stations and the total summed BFF for the Mach 0.91 condition and α=-6°, -4°, -2°, 0°, +2°, +4°, and +6°, and β=0°. Compared to the $C_{z,rms}$ value in Figure 15 for the revised station 5 loads discussed in Section III-B, Figure 30 shows that increasing the sensor density to capture the nuances of the shock motion has further reduced the z-direction BFF rms value by half. These normalized terminal shock BFF values are summarized in Table 5. For a vehicle attitude of α=0° and β=0° shown in Figure 30, the individual port BFFs in the y-direction and z-direction ($\Delta C_{y,rms}$ and $\Delta C_{z,rms}$) appear symmetric and have

nearly the same values at each port station. However, when the vehicle is pitched to nonzero values of α, Figure 30 reveals that the z-direction BFF component exhibits a dual peak that is consistent with the windward and leeward shift in the mean location of the terminal shock depicted in Figure 27. Individual and the summed BFF z-direction rms magnitudes are shown to rise with the absolute value of vehicle angle of attack.

Power spectral densities of C_y and C_z for individual port ('a' through 'p') and summed BFFs are presented in Figures 31a and 31b for the Mach 0.91 condition and for the vehicle attitude of α=4° and β=0°. The spectral content shown for z-direction BFFs in Figure 31b possess higher magnitudes than those for the y-direction in Figure 31a, which is expected due to the windward and leeward flow on the top and bottom of the vehicle due to the nonzero vehicle angle-of-attack attitude. The PSD magnitudes for each individual and summed BFF are shown to decrease significantly beyond 5-10 Hz in Figures 31a and 31b. Finer details in individual port BFF PSD magnitudes and spectral content can be found in Figures 32a and 32b, which are scaled to illustrated the 0.5 to 5 Hz frequency range. It is surprising that the spectral content of ΔC_y and ΔC_z for the individual sensors are quite different. Spectral content in Figure 32a is dominated by broad peaks in the range of 0.70 Hz to 3 Hz full-scale. However, the spectral peaks in Figure 32b in the z-direction are at 0.69 Hz full-scale, which correlates well with the spectral content of shock motion shown in Figure 26.

B. Terminal Shock BFFs Using Assumed Coarse Integration Scheme for Each Shock Array Port Station

A final observation that is important to terminal shock BFF development from wind-tunnel data, is that the results shown in Figures 30, 31, and 32 illustrate that there is a large variation in BFF magnitudes observed by each individual station on the shock array. If any one of these represented the only longitudinal station at or near a terminal shock, a wide range of BFF magnitudes could be realized if that single station was integrated over the entire shock array. This effect can be seen in Figure 33, which presents BFF PSDs that have been computed assuming that each station is integrated over the entire shock array longitudinal length. Also shown in this figure is the summed BFF as presented in Figure 31. Note that PSDs in Figure 31 are presented in a semilog format with x-axis range from 0-60 Hz full-scale while Figure 33 presents PSD on linear plot and with x-axis range of 0-10 Hz full-scale for clarity. It can be seen in Figure 33a that a large number of the port BFFs are much greater than the summed ΔC_y BFF and in Figure 33b some ΔC_z BFFs are an order of magnitude greater than the summed ΔC_z BFF. For the case of a single longitudinal station observing an oscillating terminal shock, Figure 33 suggests that a poorly chosen longitudinal sensor station can result in a large overprediction or underprediction of the BFF. Additionally, since the peak $\Delta C_{p,rms}$ associated with the terminal shock decreases with increasing Mach number as shown in Figure 17 as the terminal shock shifts downstream, the location of any terminal shock measurement station or array of stations should not be further than ½ caliber downstream of the payload shroud shoulder interface of the tangent-ogive to upper-stage. Sound test planning would utilize CFD results to guide sensor placement and Mach number choices for the test matrix.

II. Conclusions

Two wind-tunnel studies have been conducted at the NASA Langley Research Center's Transonic Dynamics Tunnel to observe the buffet environment on a heavy-lift launch vehicle with a tangent-ogive payload shroud using a 3-percent scale rigid buffet model. Initial studies revealed the presence of a strong terminal shock at Mach 0.90 that oscillated across a single longitudinal station and resulted in erroneously high buffet forcing functions (BFFs), which caused structural responses on the upper-stage engine to exceed allowable margins. The terminal shock environment was subsequently reduced through the use of unsteady FUN3D CFD results and shadowgraph movies that focused on the terminal shock motion to deduce a smaller longitudinal integration region for the terminal shock BFF. However, the need to validate this approach and to pursue further reductions prompted a second test of this configuration with 256 unsteady pressures focused on the terminal shock environment. The analysis of data from these test programs indicates:

The magnitude of a terminal shock BFF based on wind-tunnel test data can be overpredicted, underpredicted, or missed altogether due to poorly chosen sensor locations or test matrix. It is recommended that computational fluid dynamic results be used to guide unsteady pressure sensor placement and combined with shadowgraph or schlieren video system to determine the extent of shock motion in conjunction with unsteady pressure measurements.

The peak value of $\Delta C_{p,rms}$ associated with the terminal shock decreases with increasing Mach number and the terminal shock location moves aft (downstream) of the payload fairing shoulder with increasing Mach number. Therefore, it is recommended to locate terminal shock unsteady pressure transducers within ½ caliber of a tangent-ogive shoulder.

The magnitude and frequency content of a terminal shock has been shown to be impacted by the vehicle angle of attack. At low to moderate angles of attack, the terminal shock region moves forward on the leeward side of vehicle and aft on the windward side. This results in an asymmetric circumferential pressure loading as observed by unsteady sensors, especially for a coarse sensor distribution. When integrated, these azimuthally asymmetric pressure time histories can result in an overprediction of the terminal shock environment, especially when few unsteady sensors are employed at or near the terminal shock station.

Based on analysis of shock motion from shock array data, the extent of motion and thus, the terminal shock BFF integration region length, is on par with the estimate of 42 inches determined from CFD and shadowgraph videos. Shock array analysis indicates that the range of shock oscillation motion varies with vehicle attitude and ranges from 32 to 58 inches around the vehicle azimuth for this configuration.

It is recommended to place a shock array of at least 2-3 rings of unsteady sensors at the predicted location of peak terminal shock $\Delta C_{p,rms}$ in order to ensure adequate discretization of the buffet environment associated with this phenomenon.

VI. References

1. Runyan, Harry L., Jr., and Rainey, Gerald A., "Launch Vehicle Dynamics". NASA TM-X-607, December 1961.
2. Rainey, Gerald A., "Progress on the Launch-Vehicle Buffeting Problem." Journal of Spacecraft and Rockets, Volume 2, Number 3, May–June 1965.
3. Cole, Henry A., Jr., Erickson, A. L., and Rainey, A. G., "Buffeting During Atmospheric Ascent." NASA SP–8001, 1963, Revised November 1970.
4. Jones, George W., Foughner, Jerome T., Jr., "Investigation of Buffet Pressures on Models of Large Manned Launch Vehicle Configurations." NASA TN–D–1663, May 1963.
5. Fleming, E.R., "Transonic Buffeting Loads Experience at The Aerospace Corporation." The Aerospace Corporation Report No. TOR–95(5530)–6. March 1995.
6. Kabe, A.M., "Time Domain Buffet Loads Analysis." The Aerospace Corporation Report Number TOR–2007(2209)–6078. November 17, 2006.
7. Piatak, D.J., Sekula, M.K., and Rausch, R.D., "Ares Launch Vehicle Transonic Buffet Testing and Analysis Techniques." Journal of Spacecraft and Rockets. Vol. 49. No 5. September-October 2012.
8. Sekula, M. K., et al., "NASA Test Summary Document for the 3.5 Percent Ares I-X Rigid Buffet Model; Transonic Dynamic Test #599; November-December 2007," NASA TP-2015-218703, March 2015.
9. Sekula, M.K., Piatak, D.J., Rausch, R.D., "Space Launch System Program Vehicle Aerodynamic Substantiation Report for the SLS-1000X Buffet Forcing Function Database". NASA TM-2018-219830.
10. Piatak, D.J., Sekula, M.K., Rausch, R.D., Florance, J.R., and Ivanco, T.G., "Overview of the Space Launch System Transonic Buffet Environment Test Program". AIAA 2015-0557. Presented at the 53rd AIAA Aerospace Sciences Meeting, January 5-9, 2015.
11. Sekula, M.K., Piatak, D.J., Rausch, R.D., "Initial Assessment of Space Launch System Transonic Unsteady Pressure Environment". AIAA 2015-0558. Presented at the 53rd AIAA Aerospace Sciences Meeting, January 5-9, 2015.
12. Piatak, D.J., Sekula, M.K., Rausch, R.D., "Sensitivity of Space Launch System Buffet Forcing Functions to Buffet Mitigation Options". AIAA 2016-0544. Presented at the 54th AIAA Aerospace Sciences Meeting, January 4-8, 2016.
13. Cole, Stanley R., Garcia, Jerry L., "Past, Present, and Future Capabilities of the Transonic Dynamics Tunnel from an Aeroelasticity Perspective." AIAA 2000–1767, Presented at the AIAA Dynamics Specialists Conference, Atlanta, GA, April 506, 2000.
14. Cole, Stanley R., Johnson, R. Keith, Piatak, David J., Florance, Jennifer P., and Rivera, José A., Jr., "Test Activities in the Transonic Dynamics Tunnel and a Summary of Recent Facility Improvements." AIAA 2003–1958, Presented at the AIAA Dynamics Specialists Conference, Norfolk, VA, April 9–10, 2003.
15. Cole, Stanley R., Keller, Donald F., and Piatak, David J., "Contributions of the NASA Langley Transonic Dynamics Tunnel to Launch Vehicle and Spacecraft Development." AIAA 2000–1772, Presented at the AIAA Dynamics Specialists Conference, Atlanta, GA, April 5–6, 2000.

16. Brauckmann, G.J., Streett, C., Kleb, W.L., Alter, S.J., Murphy, K.J., and Glass, C.E., "Computational and Experimental Unsteady Pressures for Alternate SLS Booster Nose Shapes". AIAA 2015-0559. Presented at the 53rd AIAA Aerospace Sciences Meeting, January 5-9, 2015.
17. Alter, S.J., Brauckmann, G.J., Kleb, B., Glass, C.E., Streett, C.L., and Schuster, D.M., "Time-Accurate Unsteady Pressure Loads Simulated for the Space Launch System at Wind Tunnel Conditions". AIAA 2015-3149. Presented at the 33rd AIAA Applied Aerodynamics Conference, 22-26 June 2015.

Table 1. Space Launch System RBM TDT test section flow conditions in R134a test medium.

Mach Number	*q*, psf	*V*, ft/s	Re, /ft	Re, 1st Stage Dia.	Model Scale Buffet Bandwidth, Hz
0.8	481	441	8.47E+06	7.05E+06	0-1,002
0.9	480	499	7.47E+06	6.22E+06	0-1,002
1.0	480	546	6.92E+06	5.76E+06	0-1,004
1.2	300	653	3.66E+06	3.05E+06	0-1,059

Table 2. Shock array port longitudinal stations and azimuthal offsets.

Port ID	Model Scale Station, inches	Full Scale Station, inches	Azimuthal Offset, degrees
a	42.836	1427.867	+1
b	42.986	1432.867	-1
c	43.136	1437.867	+1
Ogive / Cylinder Interface	43.140	1438.01	N/A
d	43.286	1442.867	-1
e	43.436	1447.867	+1
f	43.586	1452.867	-1
g	43.736	1457.867	+1
h	43.886	1462.867	-1
i	44.036	1467.867	+1
j	44.186	1472.867	-1
k	44.336	1477.867	+1
l	44.486	1482.867	-1
m	44.636	1487.867	+1
n	44.786	1492.867	-1
o	44.936	1497.867	+1
p	45.086	1502.867	-1

Table 3. Rigid buffet model scaling laws.

Quantity to be Scaled	Full scale to Model scale Relationship
Pressure	$p_{fs} = p_{ms}\frac{q_{fs}}{q_{ms}}$
Force	$F_{fs} = F_{ms}\frac{q_{fs}}{q_{ms}}\left(\frac{D_{fs}}{D_{ms}}\right)^2$
Time	$T_{fs} = T_{ms}\frac{D_{fs}}{D_{ms}}\frac{V_{ms}}{V_{fs}}$
Frequency	$f_{fs} = f_{ms}\frac{D_{ms}}{D_{fs}}\frac{V_{fs}}{V_{ms}}$

Table 4. Full-scale reference trajectory conditions.

Mach Number	q, psf	V, ft/s
0.90	518.97	980.14
0.91	523.00	990.19

Table 5. Summary of Mach 0.91 terminal shock normalized BFF rms levels.

Terminal Shock BFF Description	$\Delta C_{y,rms}$	$\Delta C_{z,rms}$	$\Delta C_{y,rms}$	$\Delta C_{z,rms}$
	α=0° β=0°		α=4° β=0°	
Preliminary	0.0172	0.0161	0.0135	0.0366
Revised	0.0061	0.0058	0.0048	0.0135
Shock Array	0.0061	0.0063	0.0057	0.0069

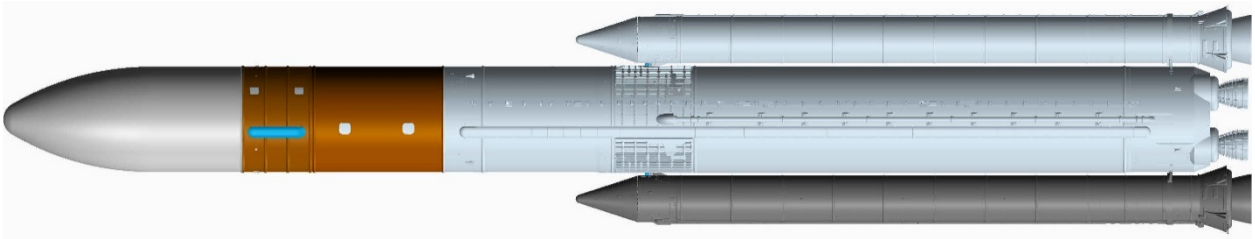

Figure 1. Space Launch System Block 1B cargo configuration (SLS-27004) with spherically-blunted tangent-ogive payload shroud.

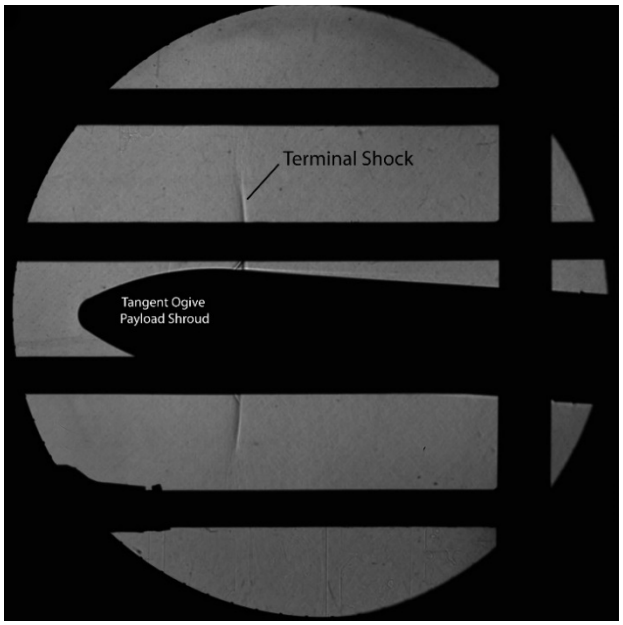

Figure 2. Shadowgraph showing terminal shock on SLS Block 1B tangent-ogive payload shroud.

Figure 3. Space Launch System Block 1B cargo vehicle configuration in the Langley Research Center Transonic Dynamics Tunnel during 2012 wind-tunnel test program.

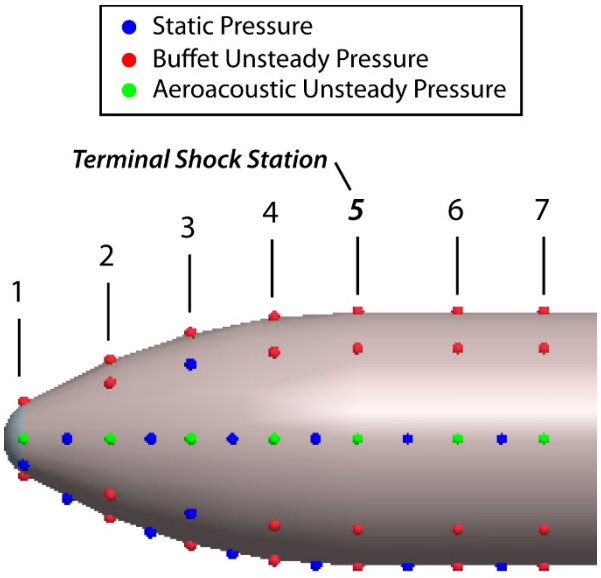

Figure 4. Unsteady pressure locations on tangent-ogive payload shroud.

Figure 5. Space Launch System Block 1B cargo vehicle configuration with terminal shock arrays in the Langley Research Center Transonic Dynamics Tunnel during 2016 wind-tunnel test program.

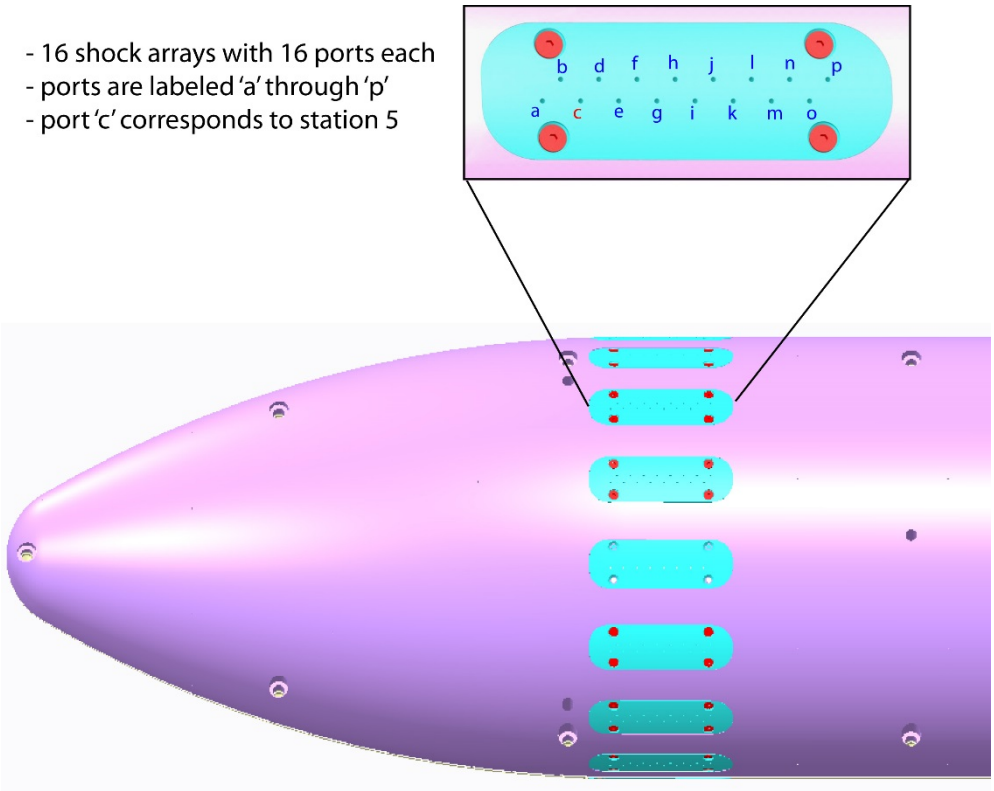

Figure 6. Pressure sensor locations for observation of terminal shock oscillation.

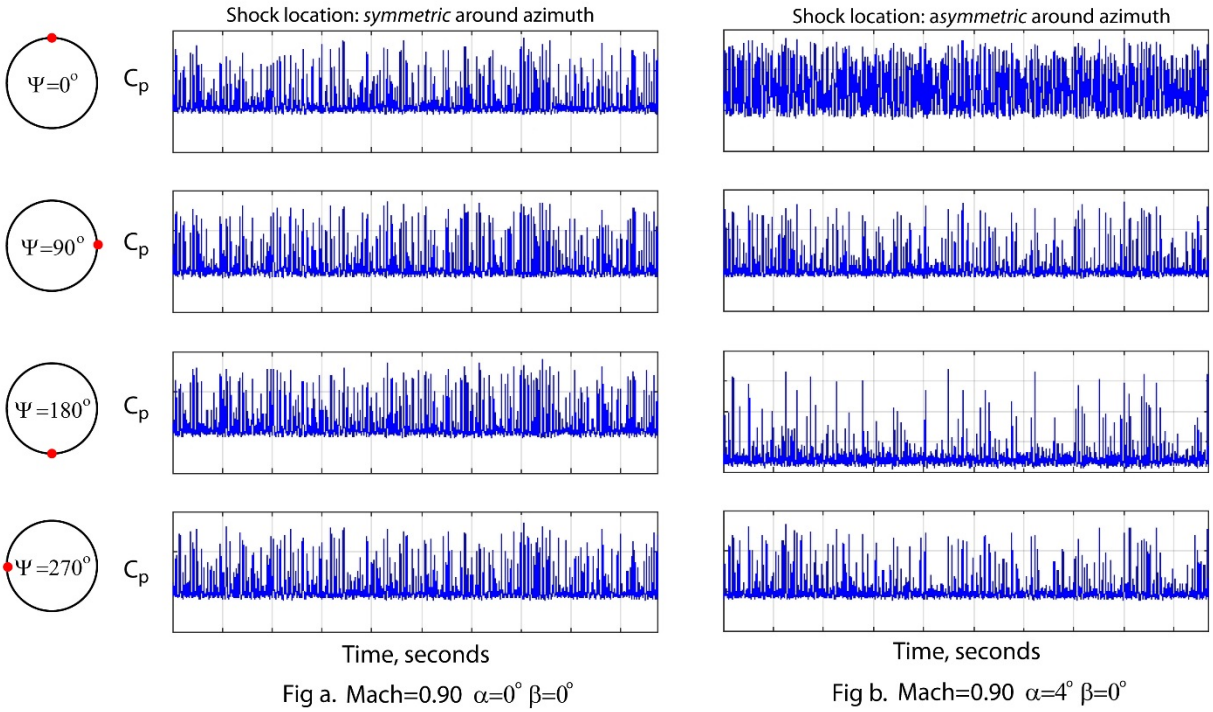

Figure 7. Pressure coefficient versus time for ring of sensors at terminal shock station for a Mach number of 0.90 and α/β=0°/0° and 4°/0°.

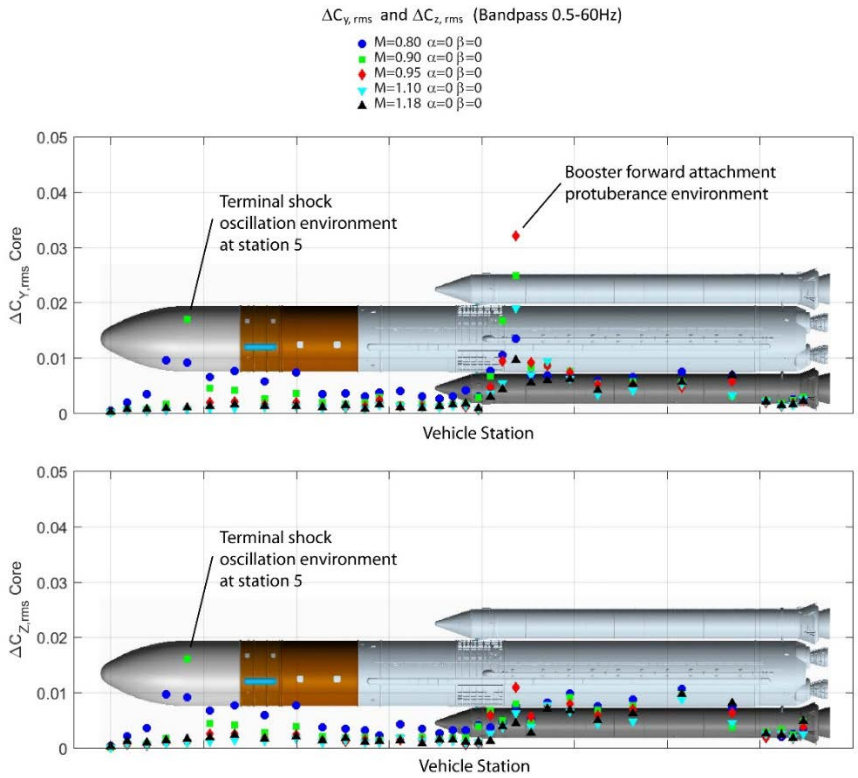

Figure 8. Preliminary normalized BFFs for SLS Block 1B cargo vehicle for M=0.80, 0.90, 0.95, 1.10, and 1.18 for α=0° and β=0°.

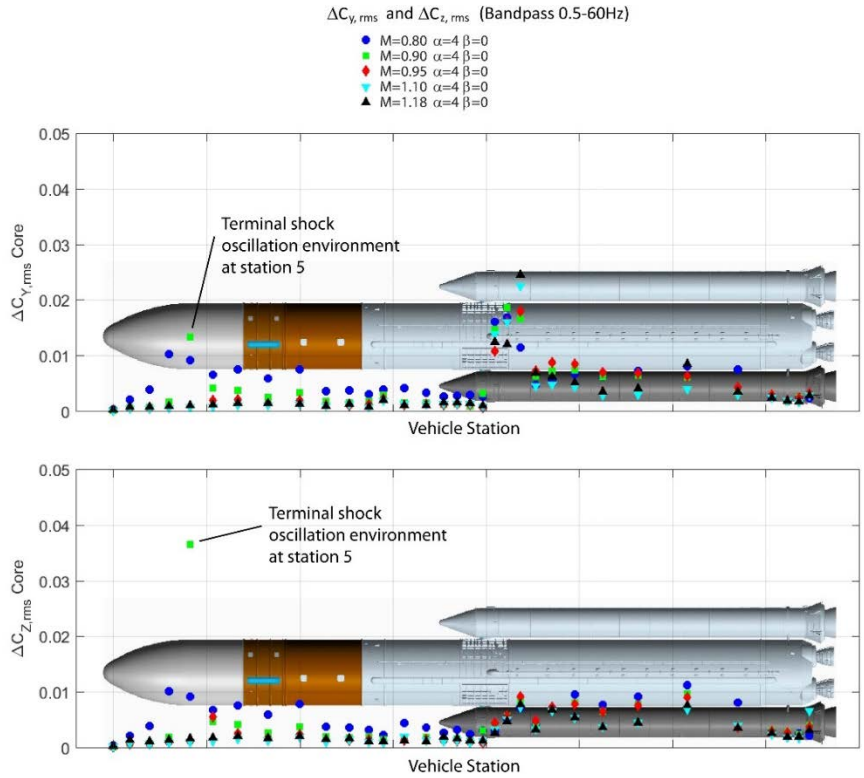

Figure 9. Preliminary normalized BFFs for SLS Block 1B cargo vehicle for M=0.80, 0.90, 0.95, 1.10, and 1.18 for α=4° and β=0°.

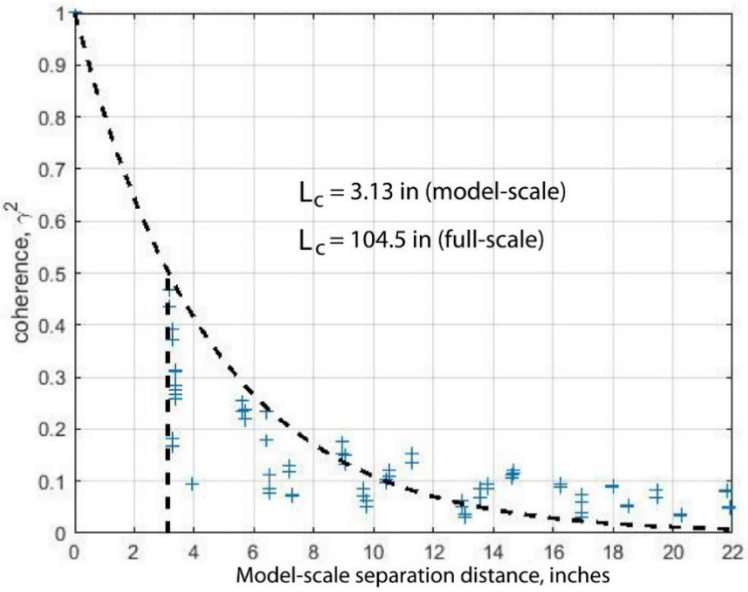

Figure 10. Magnitude-squared coherence versus longitudinal separation distance on payload shroud for Mach 0.90 and α=0° and β=0°.

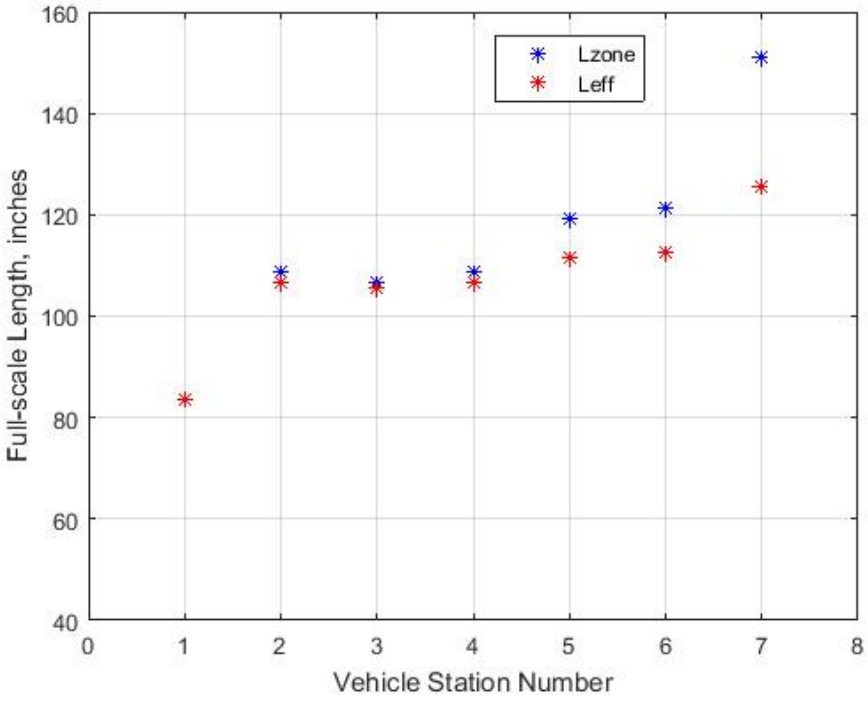

Figure 11. Zone lengths and effective longitudinal coherence lengths for stations 1 through 7 for Mach 0.90 and α=0° and β=0°.

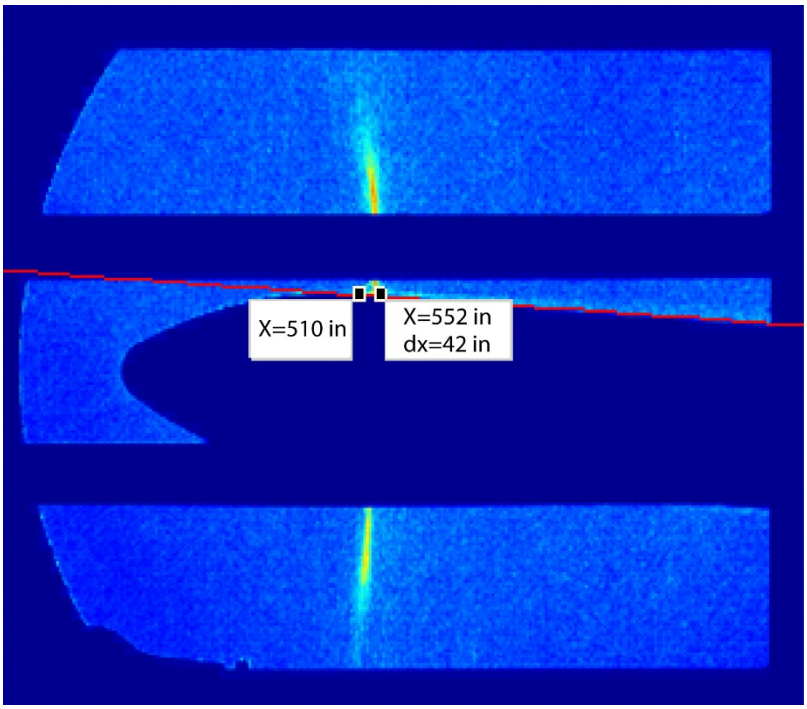

Figure 12. Standard deviation of each pixel of shadowgraph video file showing longitudinal extent of shock oscillation footprint at Mach 0.90.

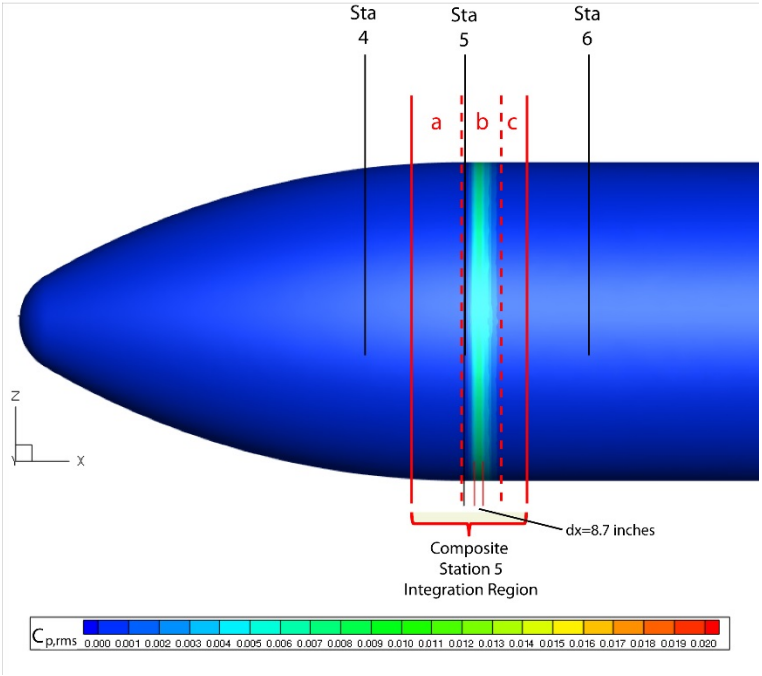

Figure 13. Pressure coefficient root-mean-square magnitude showing extent of shock oscillation from FUN3D analysis at Mach 0.90.

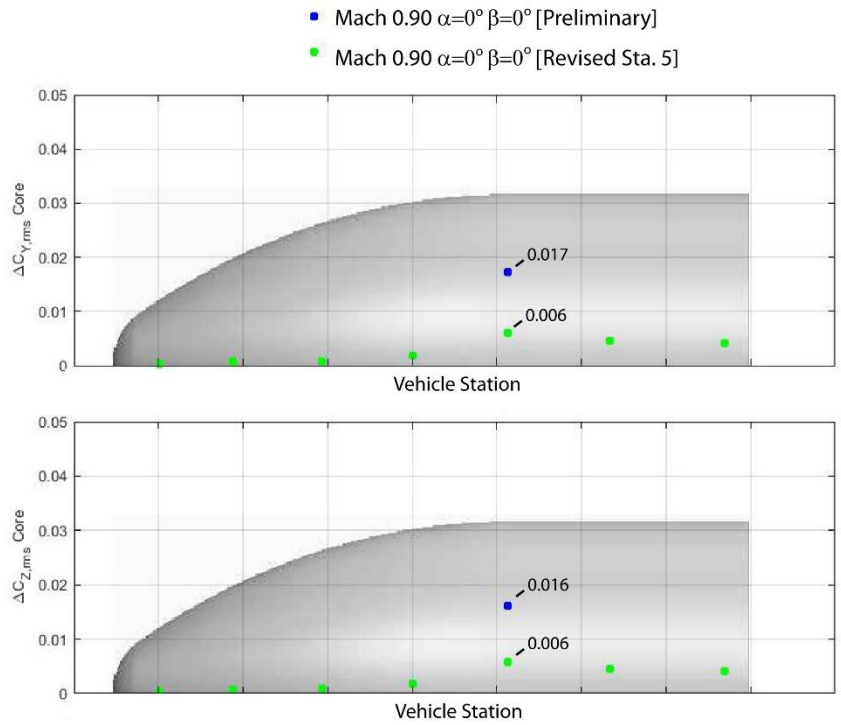

Figure 14. Preliminary and revised station 5 normalized BFFs for SLS Block 1B cargo vehicle payload shroud for M=0.90, α=0°, and β=0°.

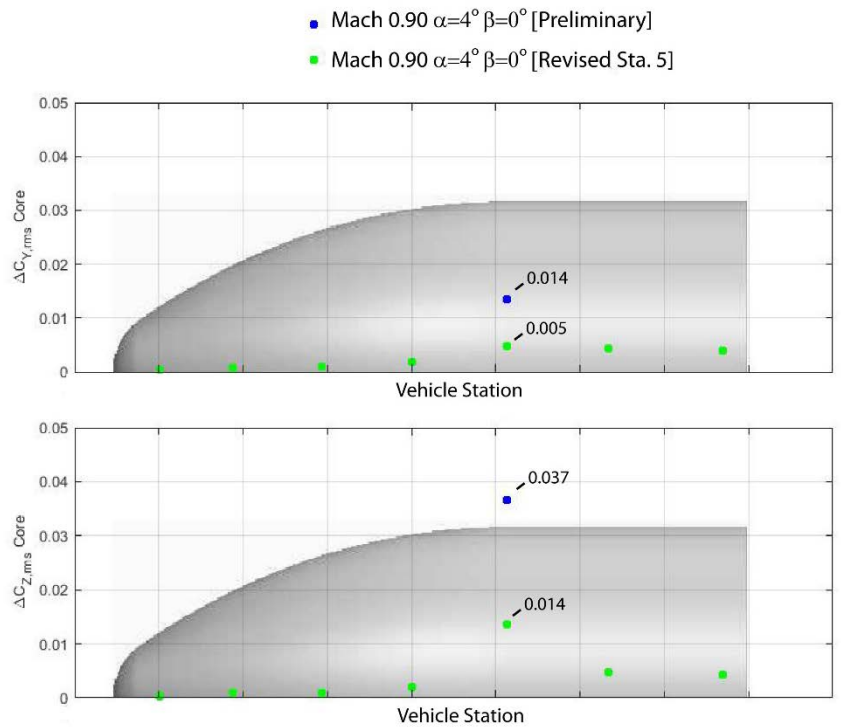

Figure 15. Preliminary and revised station 5 normalized BFFs for SLS Block 1B cargo vehicle payload shroud for M=0.90, α=4°, and β=0°.

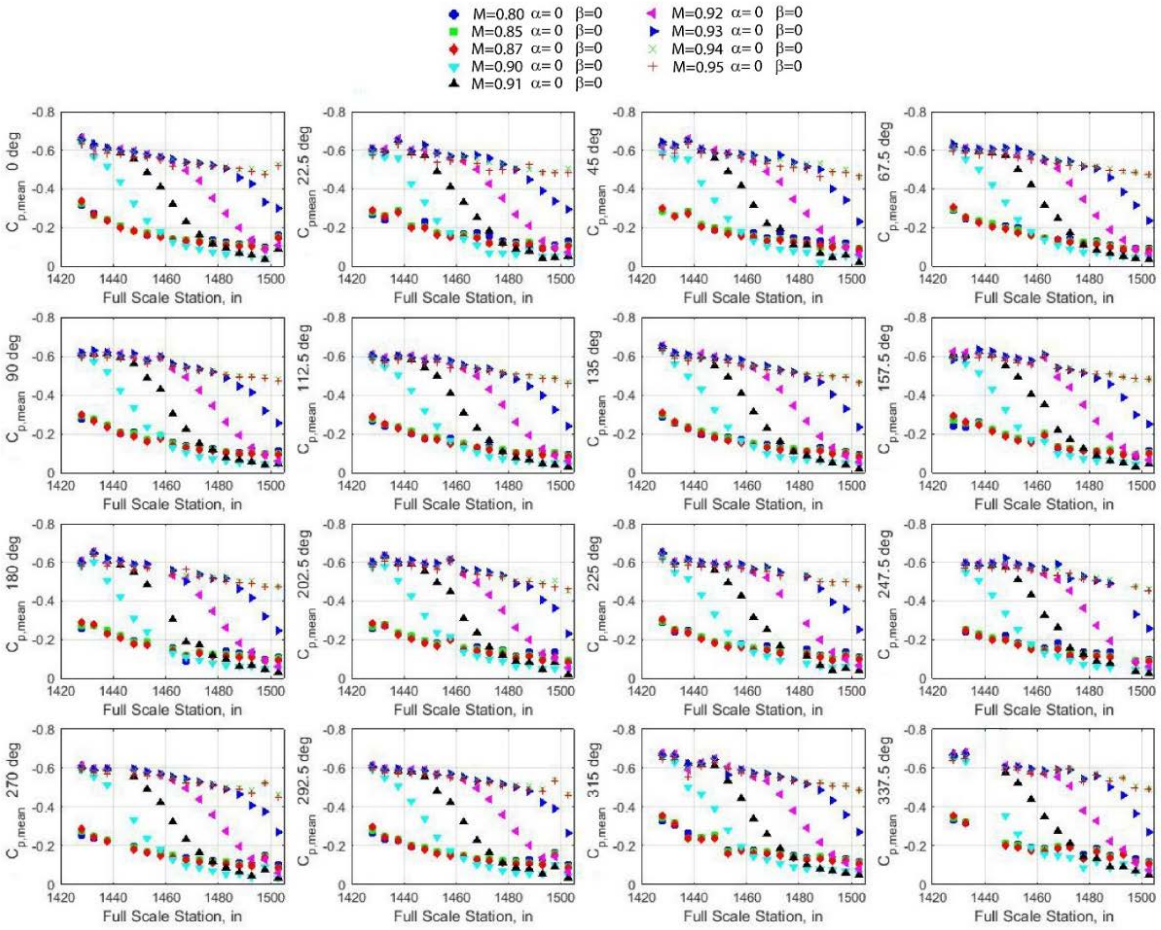

Figure 16. Mean C_p on the 16 shock arrays for Mach 0.80, 0.85, 0.87, 0.90, 0.91, 0.92, 0.93, 0.94, 0.95 and α=0°, and β=0°.

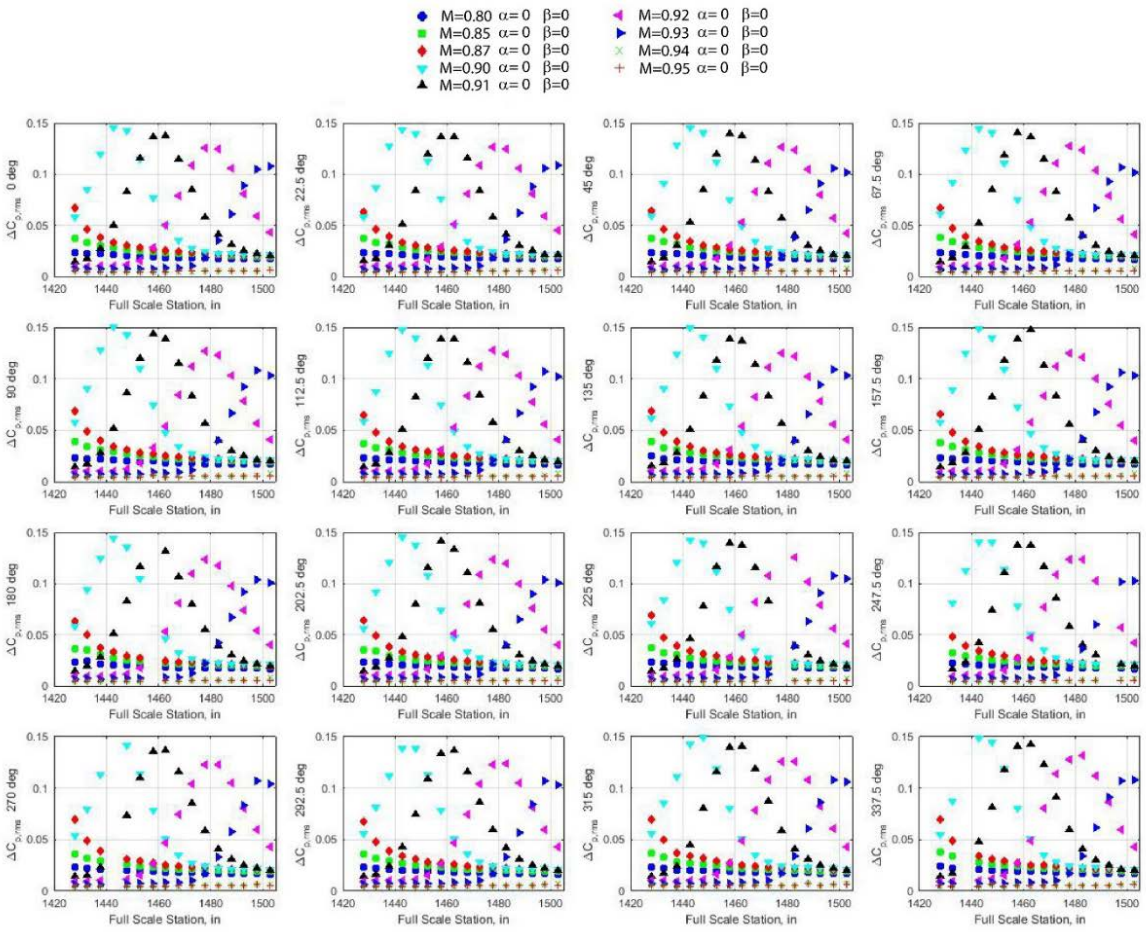

Figure 17. $\Delta C_{p,rms}$ on the 16 shock arrays for Mach 0.80, 0.85, 0.87, 0.90, 0.91, 0.92, 0.93, 0.94, 0.95 and α=0°, and β=0°.

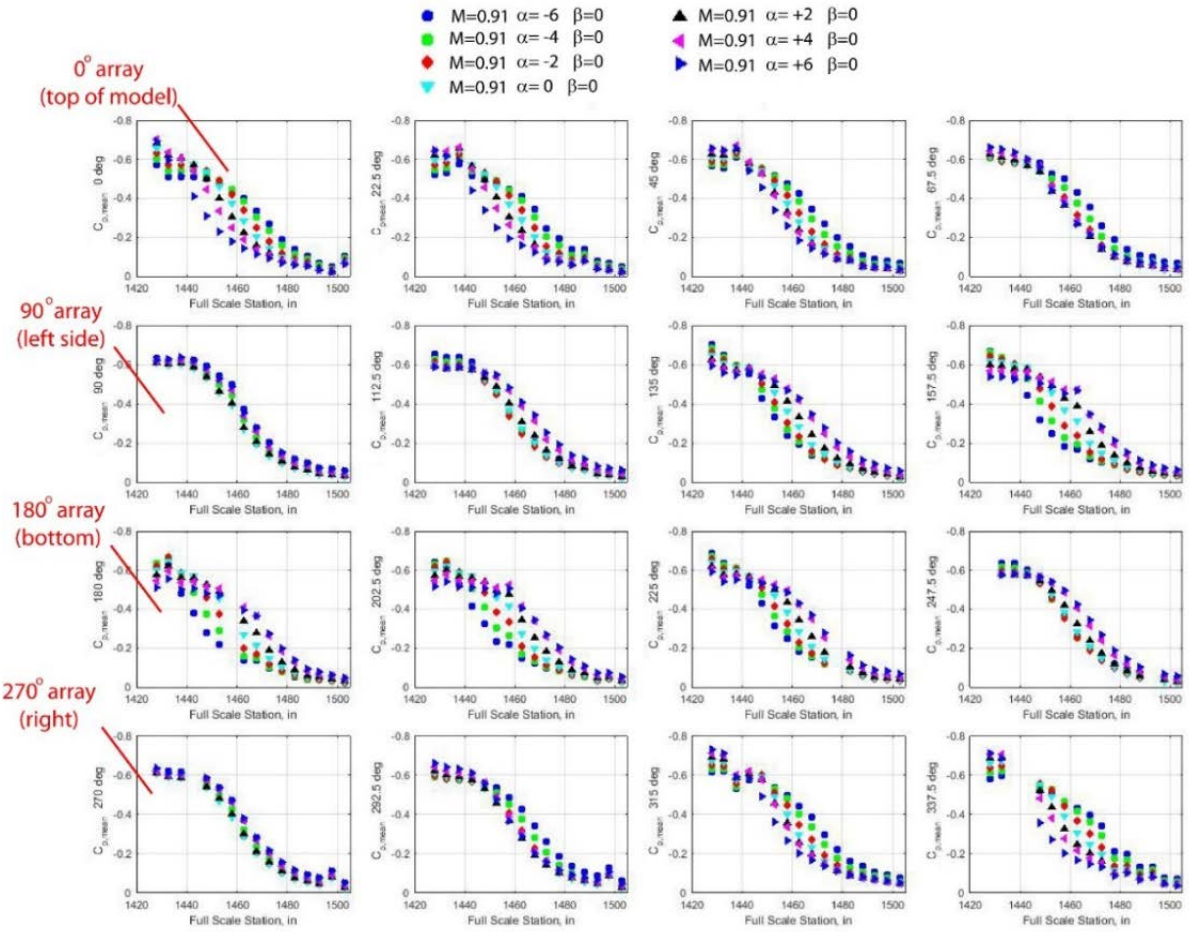

Figure 18. Mean C_p on the 16 shock arrays at Mach number of 0.91 and α=-6° to +6°, and β=0°.

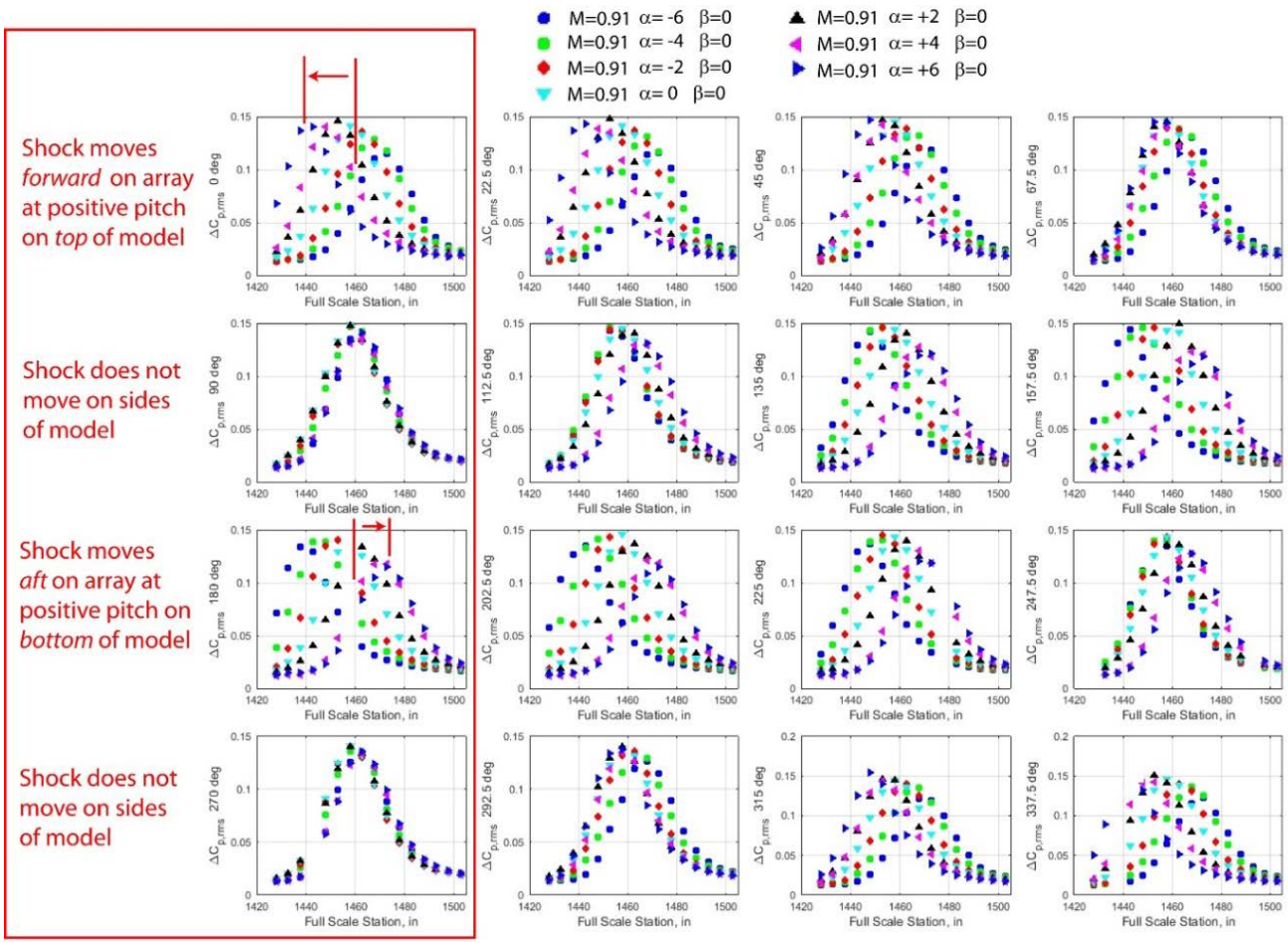

Figure 19. $\Delta C_{p,rms}$ on the 16 shock arrays at a Mach number of 0.91 and α=-6° to +6°, and β=0°.

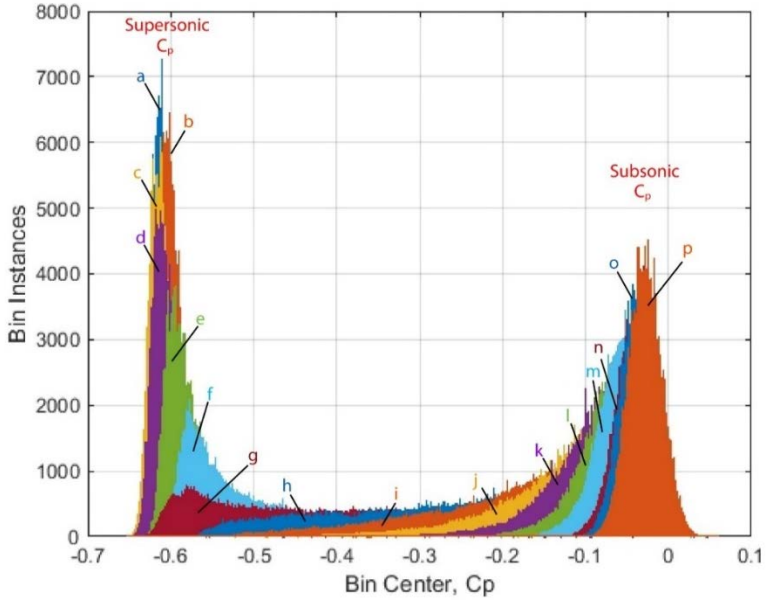

Figure 20. Histograms of pressure coefficient for all 16 sensor ports (a through p) on the shock array on left side of model (Ψ=90°) for a Mach number of 0.91 and α=0° and β=0°.

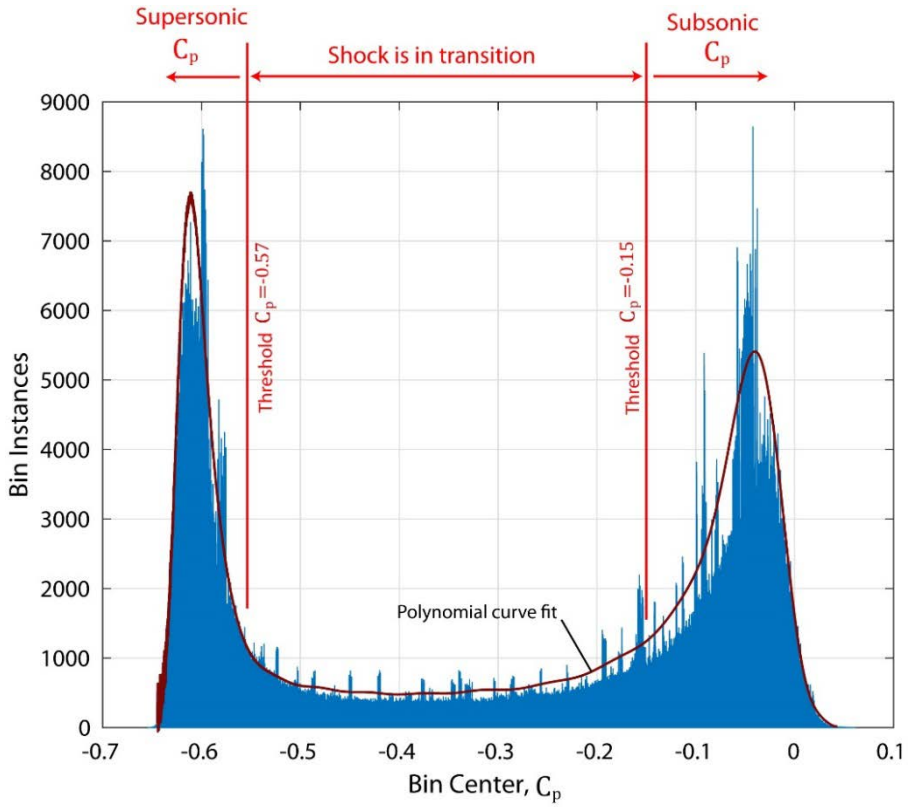

Figure 21. Summed histogram of pressure coefficient for all 16 sensor ports (a through p) on the shock array at Ψ=90° for a Mach number of 0.91 and α=0° and β=0° with supersonic and subsonic threshold C_p values identified.

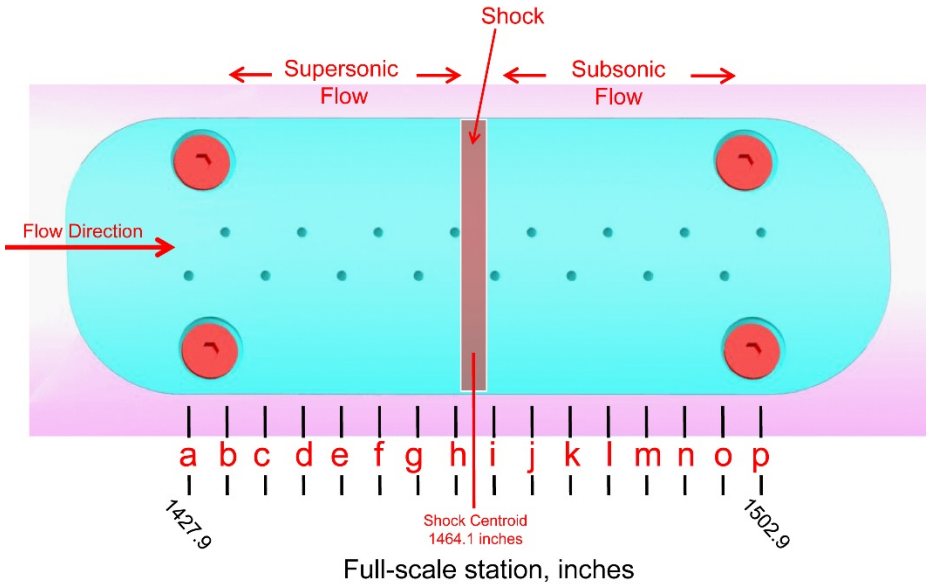

Figure 22. Shock array with port labels and shock centroid noted.

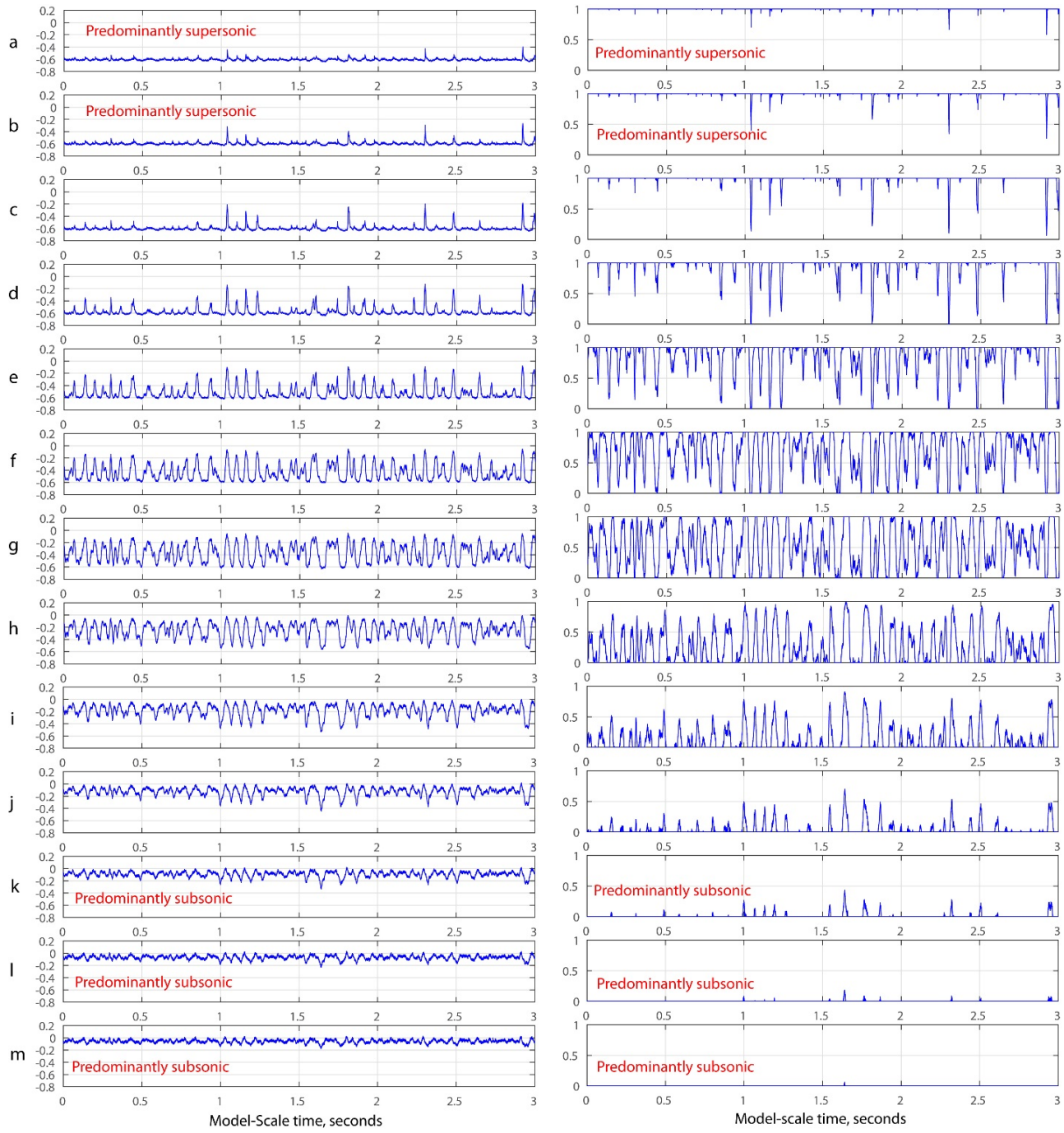

Fig a. Pressure coefficient time history.

Fig b. Shock condition time history.

Figure 23. Pressure coefficient (C_p) and shock condition (δ) time histories for the Ψ=90° shock array for a Mach number of 0.91 and α=0° and β=0°.

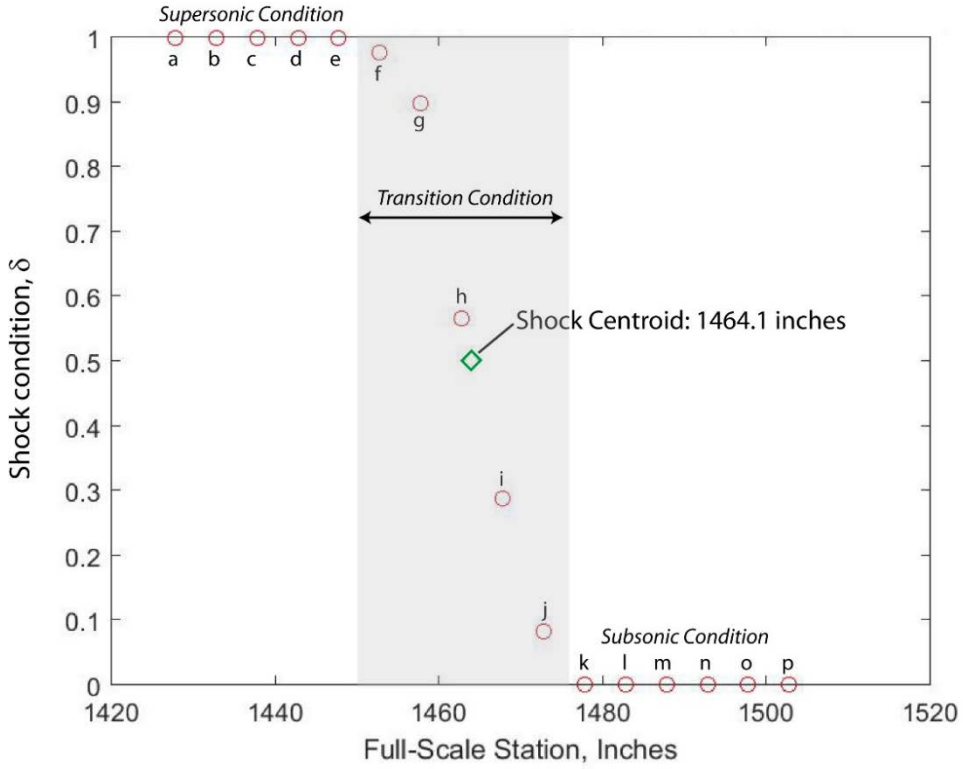

Figure 24. Interpolation of shock centroid based on shock condition values and port station locations. Model-scale time instant is 2 seconds for this figure corresponding to time histories in Figure 23a and b for Mach number of 0.91 and α=0° and β=0°.

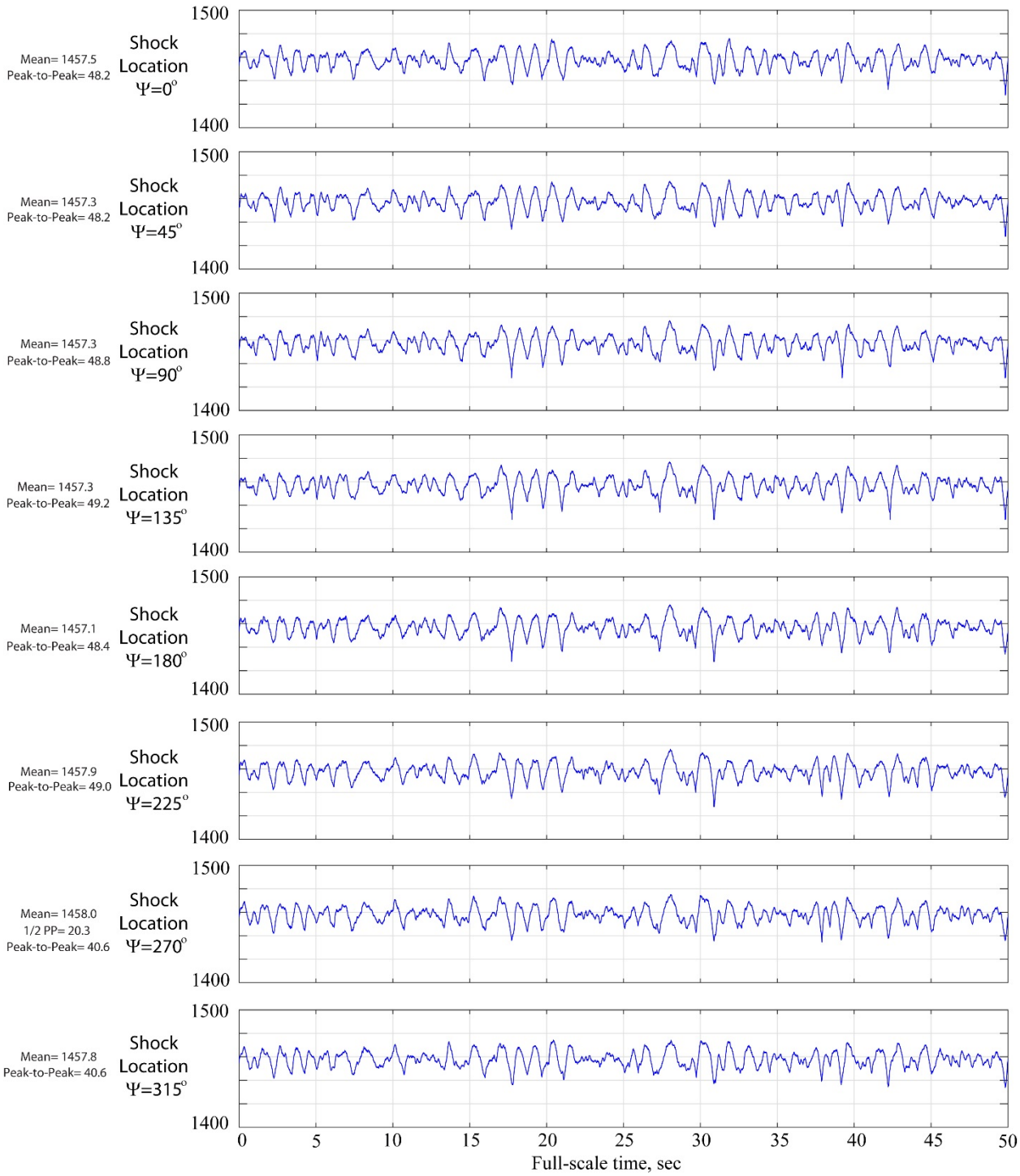

Figure 25. Shock centroid location versus full-scale time for shock arrays at Ψ=0°, 45°, 90°, 135°, 180°, 225°, 270°, and 315° for a Mach number of 0.91 and α=0° and β=0°.

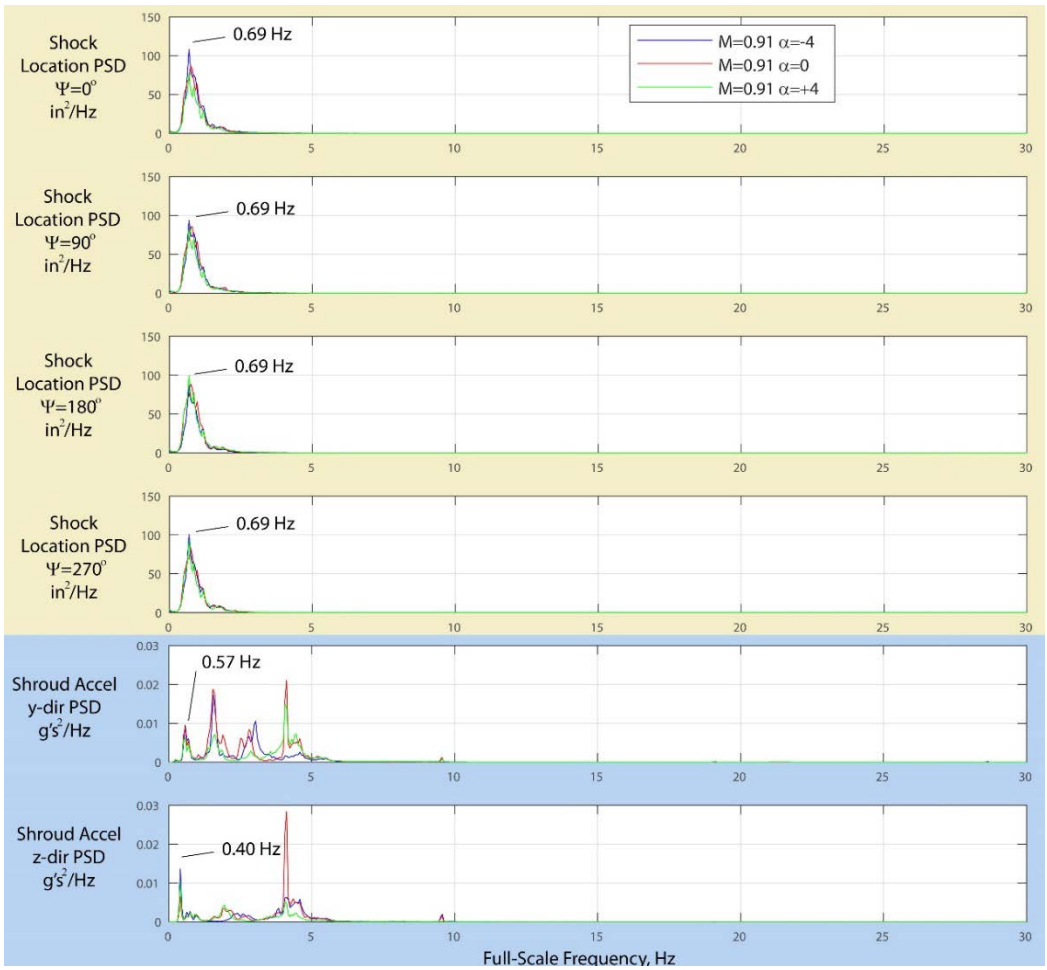

Figure 26. PSD of full-scale shock location and payload shroud accelerometers at a Mach number of 0.91 and vehicle attitude of α=-4°, 0°, and +4°, and β=0°.

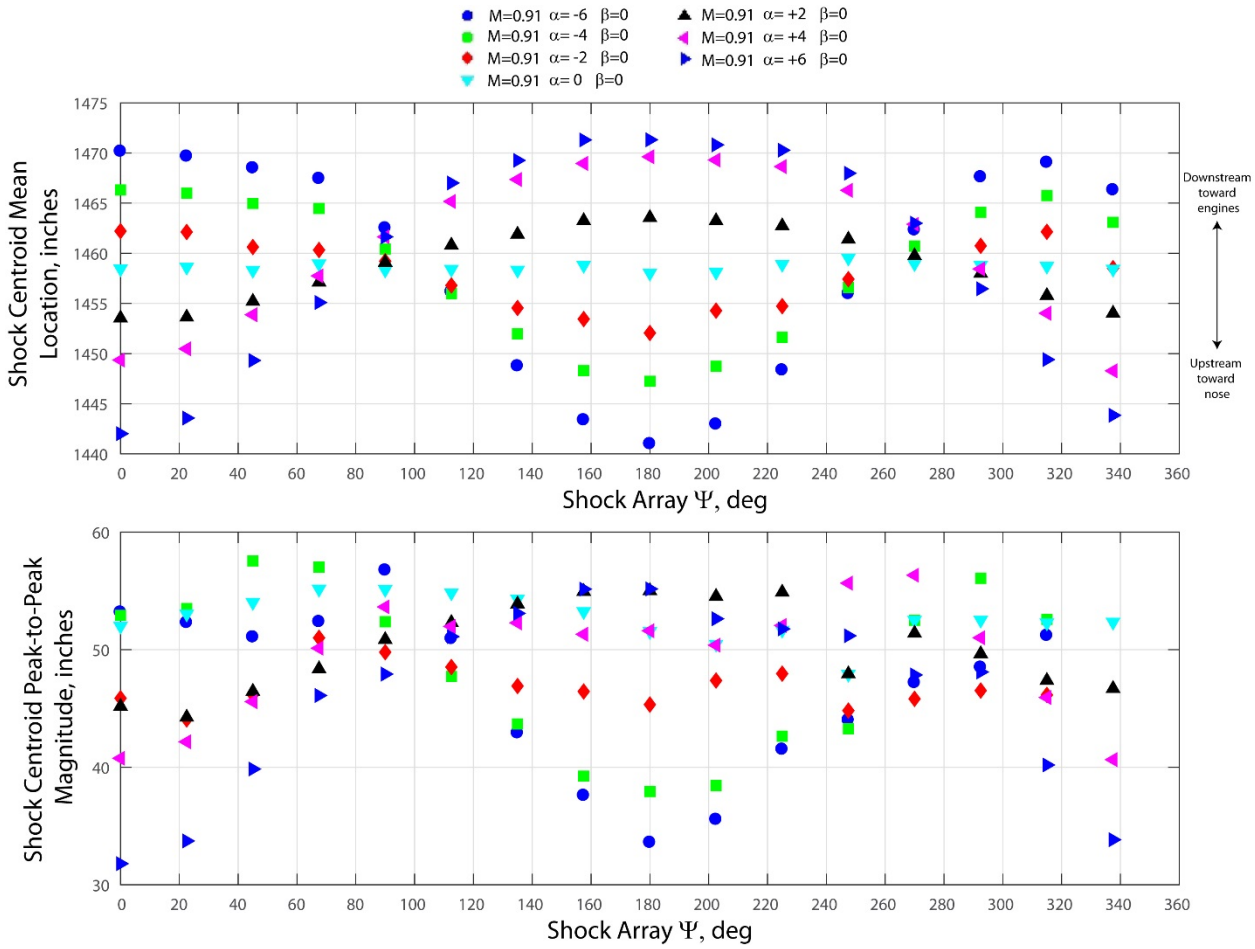

Figure 27. Shock array centroid mean and peak-to-peak magnitude values for all shock arrays at a Mach number of 0.91 and vehicle attitude of α=-6°, -4°, -2°, 0°, +2°, +4°, and +6°.

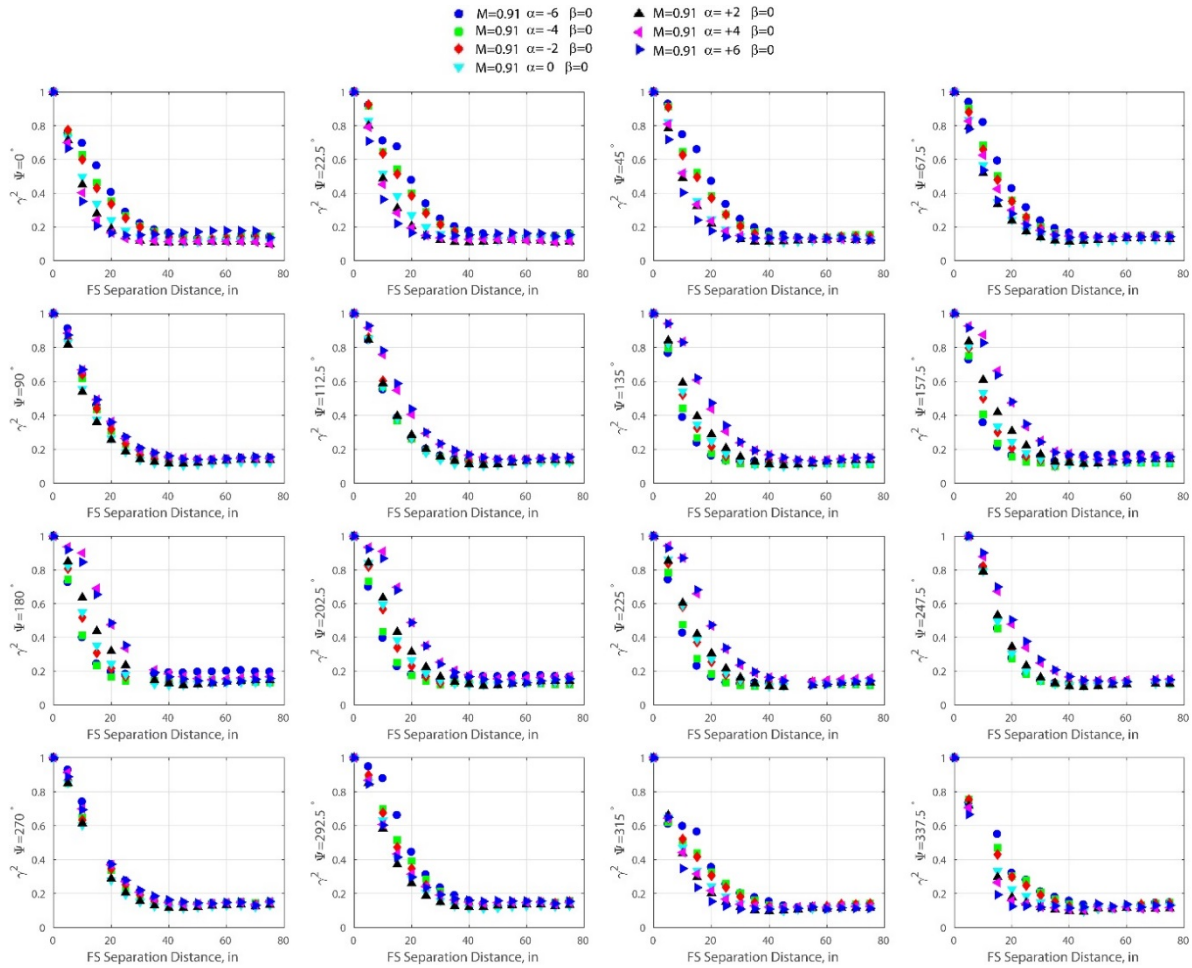

Figure 28. Longitudinal magnitude-squared coherence (γ^2) between port 'a' and each subsequent port versus full-scale sensor separation distance at a Mach number of 0.91 and α=-6°, -4°, -2°, 0°, +2°, +4°, and +6° and β=0° at each azimuthal shock sensor array.

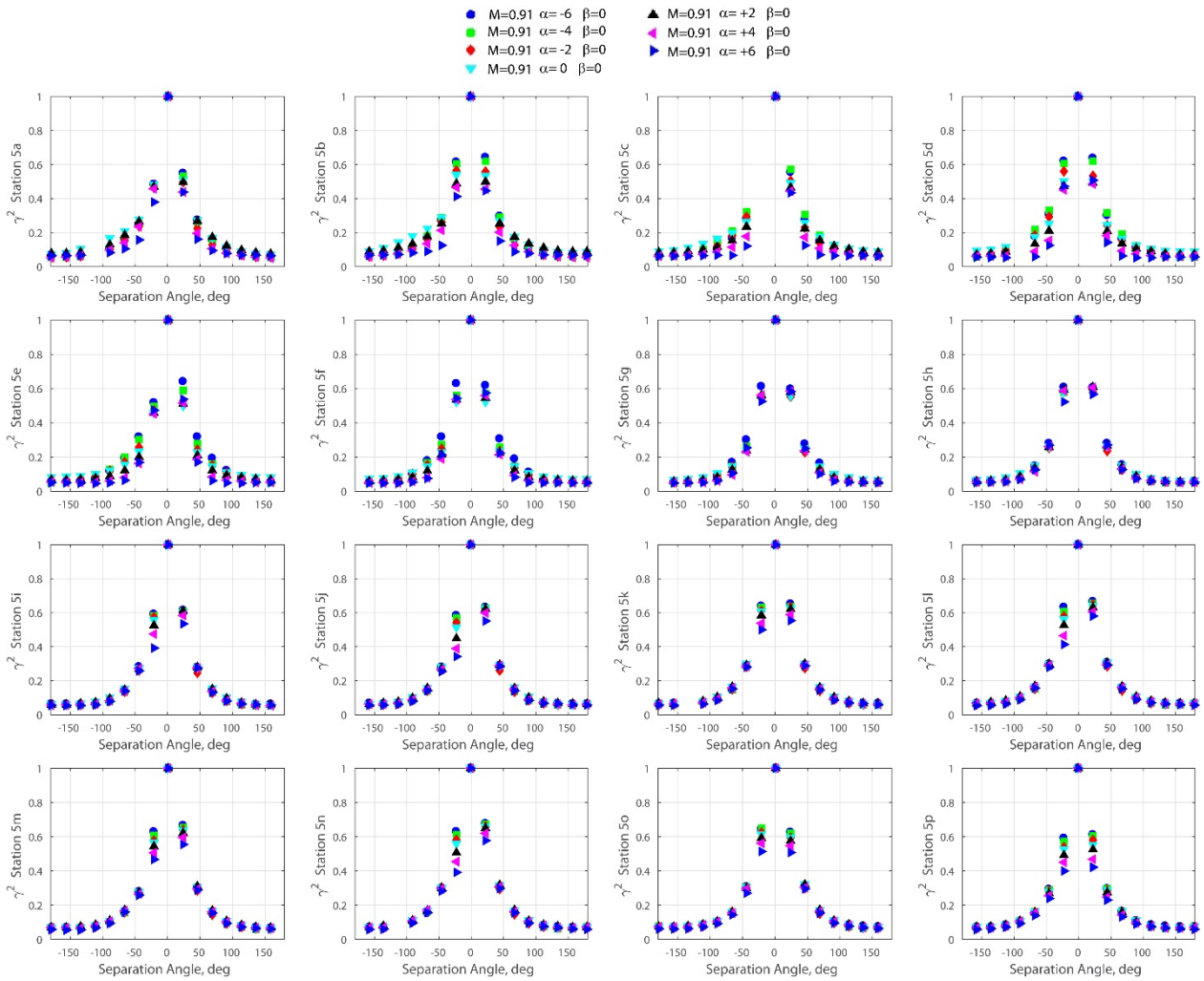

Figure 29. Azimuthal magnitude-squared coherence (γ^2) between Ψ=0° and each subsequent Ψ for each sensor station ('a' through 'p') versus sensor separation angle at a Mach number of 0.91 and α=-6°, -4°, -2°, 0°, +2°, +4°, and +6°, and β=0°.

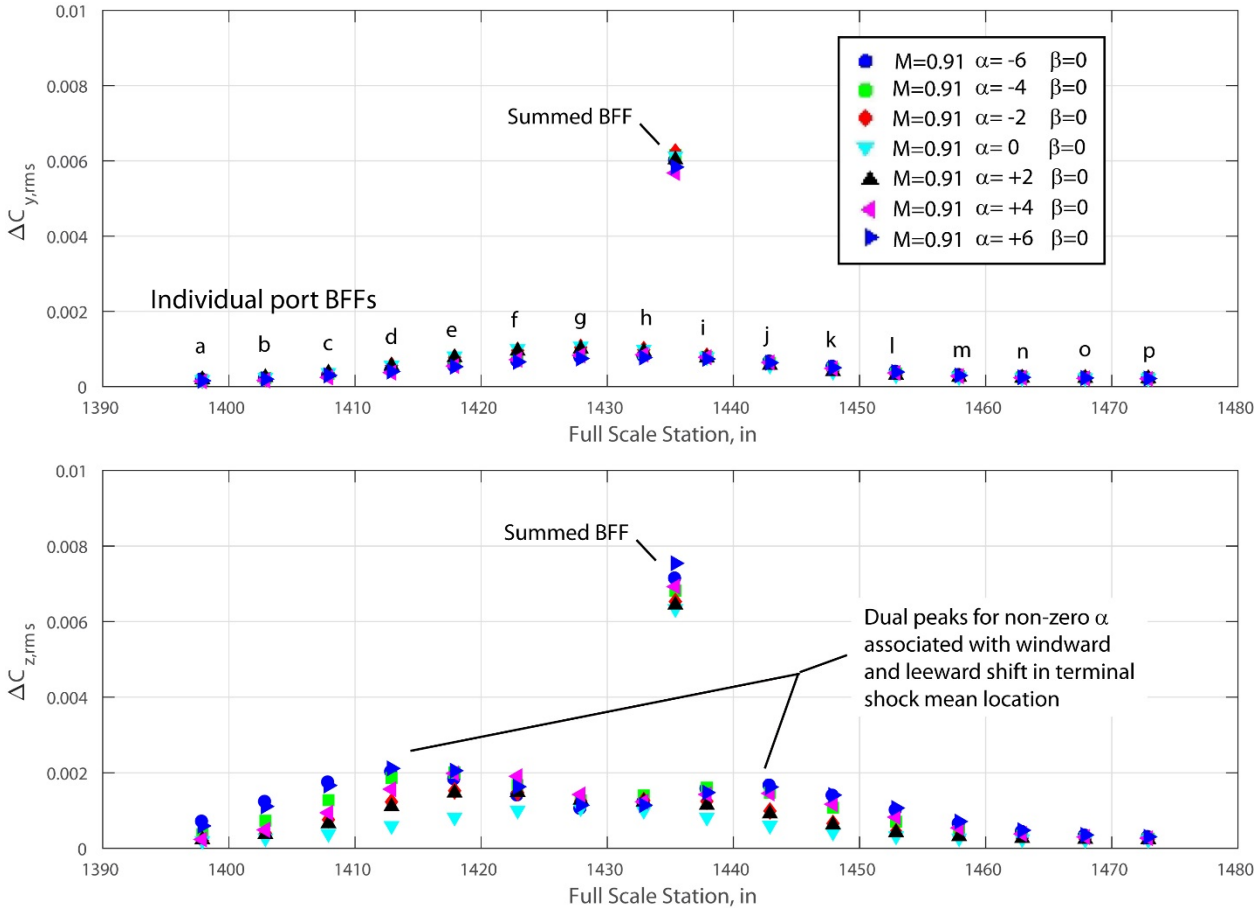

Figure 30. Individual and summed $\Delta C_{y,rms}$ and $\Delta C_{z,rms}$ BFF levels for shock arrays at M=0.91 and a vehicle attitude of α=-6°, -4°, -2°, 0°, +2°, +4°, and +6° and β=0°.

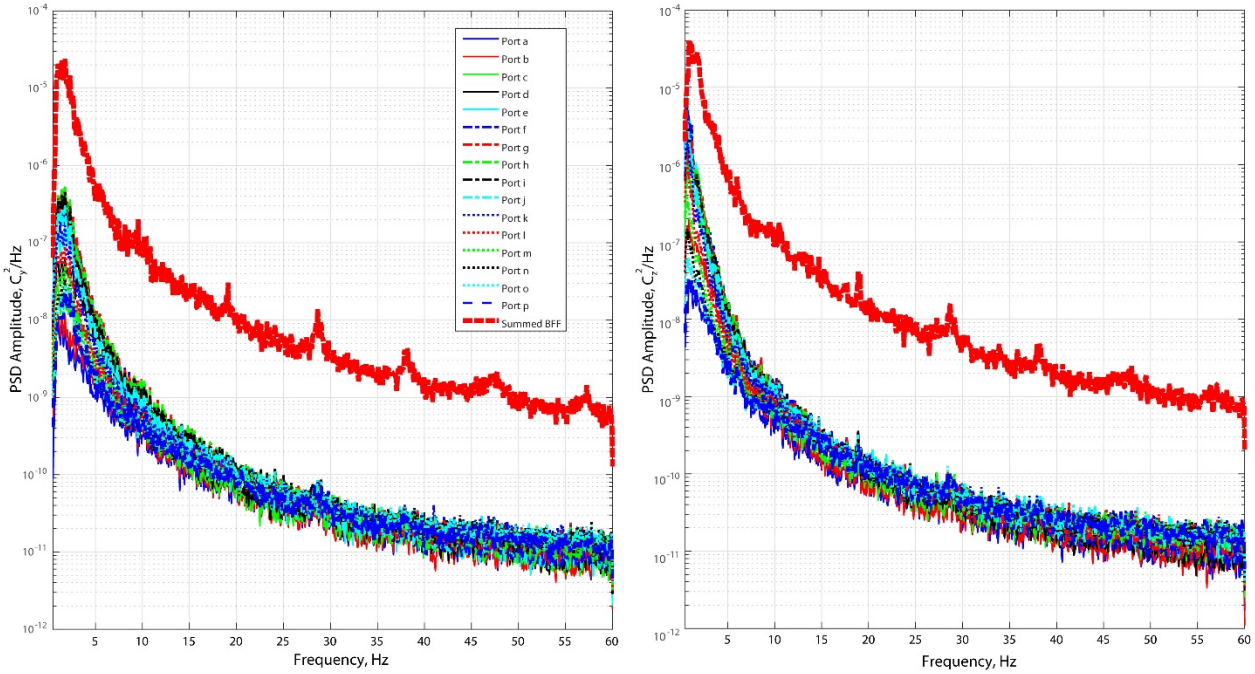

Fig a. C_y PSD amplitude versus frequency

Fig b. C_z PSD amplitude versus frequency

Figure 31. Power spectral density versus frequency for each individual port BFF and for the summed BFF for Mach 0.91 and α=4° and β=0°. Frequency axis range chosen to highlight broad spectrum full-scale buffet environment range of 0.5 to 60 Hz.

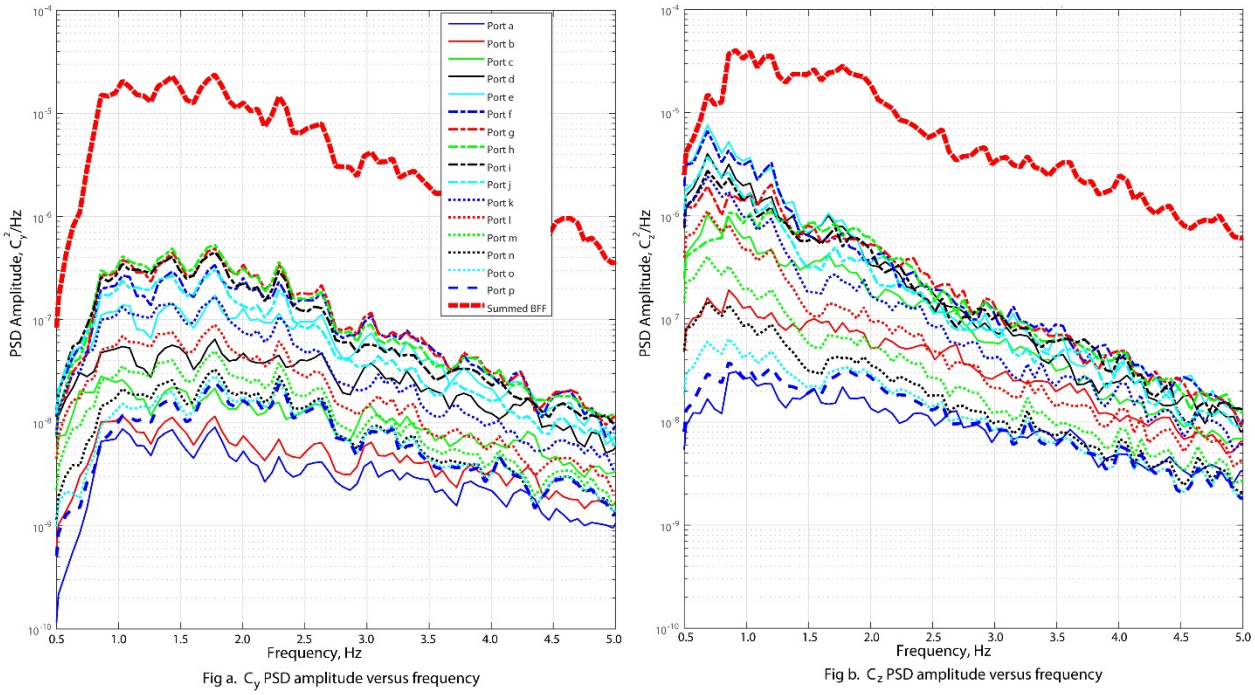

Fig a. C_y PSD amplitude versus frequency

Fig b. C_z PSD amplitude versus frequency

Figure 32. Power spectral density versus frequency for each individual port BFF and for the summed BFF for Mach 0.91 and α=4° and β=0°. Frequency axis range chosen to highlight narrowband spectrum full-scale buffet environment range of 0.5 to 5 Hz.

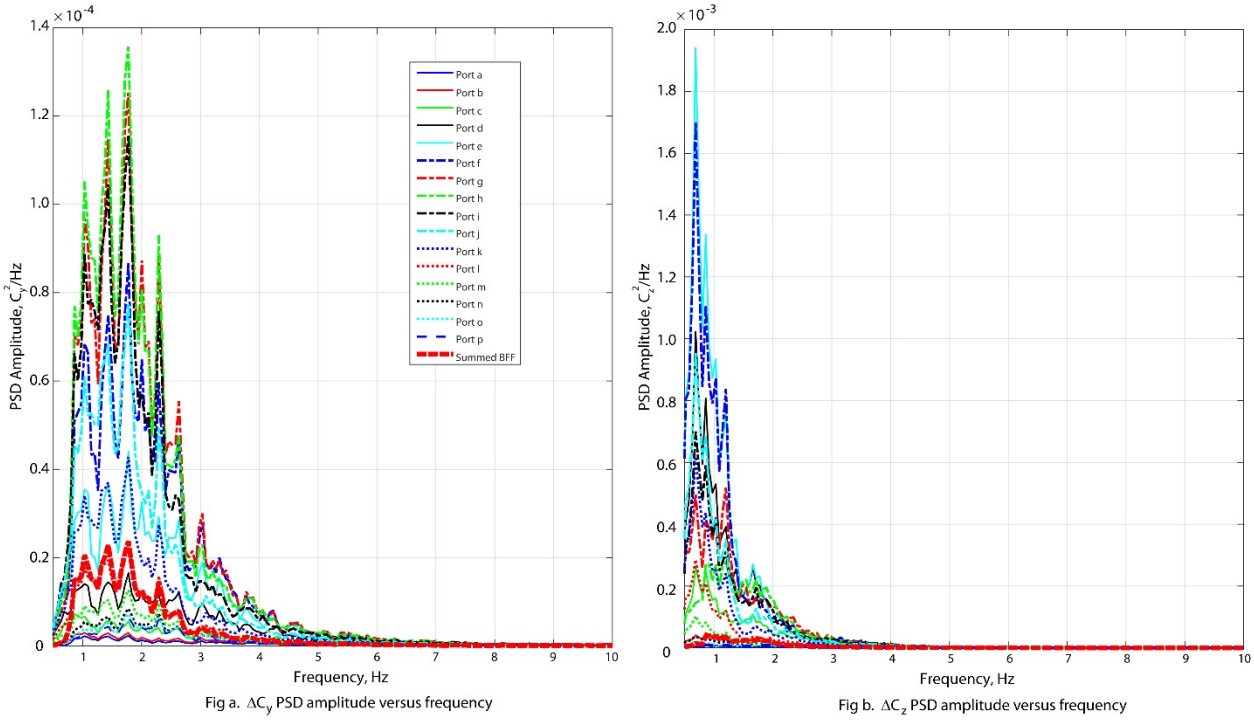

Fig a. ΔC_y PSD amplitude versus frequency

Fig b. ΔC_z PSD amplitude versus frequency

Figure 33. Power spectral density versus frequency for each port BFF integrated over entire shock array length and for the summed individual BFF found in Figure 31 for Mach 0.91 and α=4° and β=0°.